SUCNR1 signaling in adipocytes controls energy metabolism by modulating circadian clock and leptin expression

Teresa Villanueva-Carmona [1,2,†], Lídia Cedó [1,2,†], Ana Madeira [1,2], Victoria Ceperuelo-Mallafré [1,2,3], M-Mar Rodríguez-Peña [1,2], Catalina Núñez-Roa [1,2], Elsa Maymó-Masip [1,2], Maria Repollés-De-Dalmau[1,2,3], Joan Badia [4], Noelia Keiran [1,2], Mercedes Mirasierra [2,5], Carolina Pimenta-Lopes [6], Joan Sabadell-Basallote [1,2], Ramón Bosch [7], Laura Caubet [8], Joan Carles Escolà-Gil [2,9,10], José-Manuel Fernandez-Real [11,12,13], Nuria Vilarrasa [2,14], Francesc Ventura [6], Mario Vallejo [2,5], Joan Vendrell [1,2,3,*], Sonia Fernández-Veledo [1,2,*,#]

[1] Department of Endocrinology and Nutrition, Research Unit, Institut d'Investigació Sanitària Pere Virgili (IISPV) - Hospital Universitari de Tarragona Joan XXIII, Tarragona, 43005, Spain.

[2] CIBER de Diabetes y Enfermedades Metabólicas Asociadas (CIBERDEM), Instituto de Salud Carlos III, Madrid, 28029, Spain.

[3] Department of Medicine and Surgery, Universitat Rovira i Virgili (URV), Reus, 43201, Spain.

[4] Institut d'Oncologia de la Catalunya Sud, Hospital Universitari Sant Joan de Reus, IISPV, Reus, 43204, Spain.

[5] Instituto de Investigaciones Biomédicas Alberto Sols, Consejo Superior de Investigaciones Científicas/Universidad Autónoma de Madrid (CSIC/UAM), Madrid, 28029, Spain.

[6] Departament de Ciències Fisiològiques, Universitat de Barcelona, IDIBELL, Hospitalet de Llobregat, 08907, Spain.

[7] Department of Pathology, Oncological Pathology and Bioinformatics Research Group, Hospital de Tortosa Verge de la Cinta – IISPV, Tortosa, 43500, Spain.

[8] General and Digestive Surgery Service, Hospital Sant Pau i Santa Tecla, Institut d´Investigació Sanitària Pere Virgili, Tarragona, 43003, Spain.

[9] Institut d'Investigacions Biomèdiques (IIB) Sant Pau, Barcelona, 08041, Spain.

[10] Departament de Bioquímica i Biologia Molecular, Universitat Autònoma de Barcelona, Cerdanyola del Vallès, 08193, Spain.

[11] Department of Diabetes, Endocrinology and Nutrition, Institut d'Investigació Biomèdica de Girona (IdIBGi), Salt, 17190, Spain.

[12] CIBER Fisiopatología de la Obesidad y Nutrición (CB06/03/010), Instituto de Salud Carlos III, Madrid, 28029, Spain.

[13] Department of Medical Sciences, School of Medicine, University of Girona, Girona, 17004, Spain

[14] Department of Endocrinology and Nutrition, Hospital Universitari Bellvitge - IDIBELL, Hospitalet de Llobregat, 08907, Spain.

[†] These authors contributed equally to this work

[*] Senior authors: Sonia Fernández-Veledo and Joan Vendrell

Corresponding and lead contact: Sonia Fernández-Veledo (sonia.fernandez@iispv.cat)

SUMMARY

Adipose tissue modulates energy homeostasis by secreting leptin, but little is known about the factors governing leptin production. We show that succinate, long perceived as a mediator of immune response and lipolysis, controls leptin expression *via* its receptor SUCNR1. Adipocyte-specific deletion of *Sucnr1* influences metabolic health according to nutritional status. Adipocyte *Sucnr1* deficiency impairs leptin response to feeding, whereas oral succinate mimics nutrient-related leptin dynamics *via* SUCNR1. SUCNR1 activation controls leptin expression *via* circadian clock in an AMPK/JNK-C/EBPα-dependent manner. While the anti-lipolytic role of SUCNR1 prevails in obesity, its function as a regulator of leptin signaling contributes to the metabolically favorable phenotype in adipocyte-specific *Sucnr1* knockout mice under standard dietary conditions. Obesity-associated hyperleptinemia in humans is linked to SUCNR1 overexpression in adipocytes, which emerges as the major predictor of adipose tissue leptin expression. Our study establishes the succinate/SUCNR1 axis as a metabolite-sensing pathway mediating nutrient-related leptin dynamics to control whole-body homeostasis.

KEYWORDS

Adipose tissue; succinate; SUCNR1; leptin; circadian clock; obesity.

RUNNING TITLE: Succinate controls leptin expression via SUCNR1

INTRODUCTION

The concept of "signaling metabolites" in the control of metabolic homeostasis is gaining traction. The Krebs cycle substrate succinate, a pleiotropic metabolite that acts akin to hormones and cytokines through succinate receptor 1 (SUCNR1), is one example of this new class of metabolites[1,2]. SUCNR1 has a broad expression in tissues and is highly abundant in white adipose tissue (WAT)[3,4]. It was generally assumed that SUCNR1 is functionally inactive in healthy tissues, and for many years SUCNR1 was investigated mainly in inflammatory-related conditions[5–8], in particular those associated with chronic hypersuccinemia[9–12]. Recent studies, however, have described that extracellular succinate transiently increases in response to physiological stimuli including exercise[13], cold exposure[14] or food ingestion, as we recently reported[15]. Succinate thus emerges as a reporter of both tissue stress and metabolism, opening up the possibility of its involvement in other metabolic functions as a hormone-like metabolite[1]. Indeed, "succinate sensing" by SUCNR1 may constitute part of the metabolite-sensing machinery governing energy homeostasis.

Adipose tissue is central in the regulation of whole-body energy homeostasis. WAT functions both as a key energy reservoir and an endocrine organ by producing an array of secreted factors that act centrally and peripherally to control metabolic activity[16]. Chief among these factors is leptin, which controls adipose tissue mass by regulating food intake through signaling in the central nervous system (CNS)[17,18]. Circulating levels of leptin are proportional to fat stores[19,20] and rise after feeding[21]. The discovery of leptin in 1994 led to a paradigm shift in our conception of adipose tissue, but how adipocytes regulate leptin production remains enigmatic. Many studies have attempted to elucidate leptin action in both peripheral and CNS tissues[17,22], and to understand leptin resistance in obesity[23,24]. So far, only a few factors have been described as regulators of leptin expression and secretion, including insulin[25–27], glucocorticoids[26–28], and catecholamines[26,29,30].

Though SUCNR1 is highly expressed in adipocytes[3], thus far the only function ascribed to it in this tissue is the inhibition of lipolysis, which is important in obesity[3,4,31]. As with other G protein–coupled receptors (GPCRs), SUCNR1 transmits signals through multiple pathways in a cell-specific manner[32], yet our knowledge of the signaling properties of this receptor is limited. SUCNR1 engagement in white adipocytes has been associated with the $G\alpha_i$-cAMP signaling transduction pathway[4], and the anti-lipolytic action of the succinate/SUCNR1 axis could provide a good explanation for the moderate lean phenotype observed in whole-body *Sucnr1*-knockout (KO) mice under standard dietary conditions[3]. However, discrepant results have been reported in *Sucnr1*-KO mice fed obesogenic diets[3,33]. Given that energy homeostasis requires multi-tissue

crosstalk, the use of cell-specific KO approaches is invaluable to decipher tissue-specific gene functions. This strategy has led to a better understanding of the key role of the succinate/SUCNR1 axis in macrophage immune response in obesity[34].

Here, we investigated the contribution of the succinate/SUCNR1 axis to adipose tissue physiology by generating mice lacking *Sucnr1* specifically in adipocytes. Metabolic phenotyping of these mice under standard dietary conditions and after diet-induced obesity, coupled with *in vitro* and human studies, demonstrates that the succinate/SUCNR1 axis is a novel regulator of leptin production in adipocytes. Our study supports the novel concept that SUCNR1 is a key metabolic sensor in energy homeostasis.

RESULTS

Conditional adipocyte deletion of *Sucnr1* reduces adipose mass and improves systemic metabolic health

We selectively inactivated *Sucnr1* in murine adipocytes. Mice carrying the floxed *Sucnr1* allele containing two loxP sites flanking exon 2[3] were bred with transgenic mice expressing Cre recombinase driven by the adipocyte-specific *Adipoq* promoter, generating *Sucnr1*$^{fl/fl}$ *Adipoq*-Cre$^{+/-}$ mice (hereafter referred to as Ad-*Sucnr1* KO mice). Cre-negative *Sucnr1*$^{fl/fl}$ mice (*Sucnr1*$^{fl/fl}$ *Adipoq*-Cre$^{-/-}$) served as controls (referred to as *Sucnr1*$^{fl/fl}$ mice) (Figures S1A and S1B). Ad-*Sucnr1* KO mice were born at a normal Mendelian ratio and were viable, and no gross morphological differences were observed between genotypes. As expected, *Sucnr1* expression was negligible in all the examined fat depots of Ad-*Sucnr1* KO mice when compared with *Sucnr1*$^{fl/fl}$ mice, whereas no changes were observed in other tissues such as liver and spleen (Figure S1C). *Sucnr1* expression in *Sucnr1*$^{fl/fl}$ mice was lower in brown adipose tissue (BAT) than in WAT (Figure S1D).

Body weight was higher in 8-week-old Ad-*Sucnr1* KO mice than in age-matched *Sucnr1*$^{fl/fl}$ littermates on normal chow diet (NCD), but these differences disappeared at 30 weeks of age (Figures 1A and 1B), suggesting that Ad-*Sucnr1* KO mice show resistance to age-related body weight gain. Indirect calorimetry analysis at 12 weeks of age revealed similar energy expenditure (EE) between genotypes (Figure S2A); however, Ad-*Sucnr1* KO mice had a significantly higher food intake during the dark (active) phase, which was independent of body weight (Figure 1C), and a significantly higher respiratory exchange ratio (RER) (Figure 1D). No differences were observed in locomotor activity between genotypes (data not shown). Similar results were obtained at 20 weeks of age (Figures S2B–D). Body composition analysis by quantitative magnetic resonance imaging (qMRI) at 12 weeks of age showed that the total amount of subcutaneous (scWAT) and visceral (vWAT) fat was significantly lower in Ad-*Sucnr1* KO mice than in *Sucnr1*$^{fl/fl}$ mice (Figure 1E), whereas muscle mass was similar (Figure S2E). The lower adiposity in Ad-*Sucnr1* KO mice was also evident at 29 weeks of age (Figure S2F). In line with this, histology of adipose tissue revealed a significantly smaller adipocyte area of inguinal (iWAT) and epididymal (eWAT) WAT in Ad-*Sucnr1* KO mice (Figure 1F). No overt histological differences were noted between genotypes in other metabolic tissues (Figure S2G). Consistent with the adipose tissue phenotype, glucose tolerance (Figure 1G) and insulin sensitivity (Figure 1H) was significantly better in Ad-*Sucnr1* KO mice than in *Sucnr1*$^{fl/fl}$ mice.

While the lower fat mass in *Ad-Sucnr1* KO mice could be explained by the known anti-lipolytic function of SUCNR1[3,4] (Figure S2H), long-term inhibition of lipolysis *in vivo* with atglistatin

(ATGLi, a specific inhibitor of adipose triglyceride lipase) had no significant impact on body weight gain as expected[35] (Ad-*Sucnr1* KO-Control=9.07±4.98% *vs* Ad-*Sucnr1* KO-ATGLi=5.22±3.08%). There were neither substantial changes on adipocyte size (only a small increase was detected in iWAT, Figure S2I) and glucose tolerance (Figure S2J) in *Ad-Sucnr1* KO mice on NCD. This agrees with previous findings demonstrating that general GPCR-mediated lipolysis is not perturbed in global *Sucnr1* KO mice under steady-state conditions[3], and points to alternative mechanisms underlying the metabolically favorable phenotype of Ad-*Sucnr1* KO mice.

The reduced adipose mass in Ad-*Sucnr1* KO mice was associated with a marked increase in the expression of the BAT activation marker UCP1 in WAT (Figure 1I) but not in BAT (Figure S2K). It was previously reported that the differentiation ability of adipocyte precursors to white adipocytes was unaffected by global *Sucnr1* deletion[3]. We found that adipose-derived stem cells from Ad-*Sucnr1* KO mice displayed a more robust brown adipocyte differentiation capacity than equivalent cells from control mice, as revealed by the higher expression of browning-related genes (Figure 1J and 1K). This was not related to differences in *Sucnr1* expression in adipocyte precursors (Figure 1L). Induction of WAT browning correlated with the accumulation of succinate, which has been previously described as a thermogenic and browning agent[14,36], in *ex vivo* adipocyte explants from *Sucnr1*-deficient WAT (Figure 1M). Overall, these results demonstrate that conditional *Sucnr1* deletion in adipocytes reduces adiposity (but not body weight) and improves glucose homeostasis by a mechanism that could be dependent on WAT browning.

Mice with conditional adipocyte deletion of *Sucnr1* develop hepatic steatosis and glucose intolerance on high-fat diet

Obesity induces elevated adipose tissue *SUCNR1* expression in both mice and humans[34]. To examine the role of adipocyte *Sucnr1* in the context of overnutrition, mice were placed on a high-fat diet (HFD) for 12 weeks. Contrary to the results on NCD, body weight gain (Figure 2A and 2B) was similar between genotypes after this period. Analysis of fat mass revealed the opposite phenotype to that seen on NCD, with a trend for greater fat mass in Ad-*Sucnr1* KO mice than in *Sucnr1*$^{fl/fl}$ mice (Figure 2C). Comparative analyses of energy parameters revealed a similar EE (Figure 2D), but a lower food intake during the light phase (Figure 2E) and a lower RER (Figure 2F) in Ad-*Sucnr1* KO mice. The change in fuel preference towards lipids is in agreement with the evident glucose intolerance (Figure 2G) and insulin resistance (Figure 2H) in the absence of significant changes in adipose tissue morphology (Figure 2I). Furthermore, HFD-induced hepatic steatosis was more severe in Ad-*Sucnr1* KO mice (Figure 2I). This might explain why no differences were detected in plasma triglycerides and non-esterified fatty acids between

genotypes (Figure 2J) despite the known negative control of lipolysis by SUCNR1[3,4]. Indeed, inhibition of lipolysis with ATGLi for two weeks ameliorated the HFD-induced hepatic steatosis in Ad-*Sucnr1* KO mice (Figure 2K), which was accompanied by improved glucose tolerance (Figure 2L). Collectively, the data indicate that, in response to overnutrition, mice with adipocyte-specific deletion of *Sucnr1* have ectopic fat deposition in liver and glucose homeostasis disturbances. The opposite metabolic phenotype of Ad-*Sucnr1* KO mice during nutritional challenge seems to be mostly dependent on the anti-lipolytic effect of SUCNR1.

Mice with conditional adipocyte deletion of *Sucnr1* develop a bone mass phenotype

To better understand the greater body weight of young Ad-*Sucnr1* KO mice despite the lower fat mass (and similar skeletal muscle mass), we assessed whether *Sucnr1* loss in adipocytes might indirectly impact skeletal mass, which accounts for ~5% of total body weight in mice[37]. Microcomputed tomography analysis of tibias showed that adipocyte deletion of *Sucnr1* changed the cortical bone mass. Cortical bone volume was significantly higher in Ad-*Sucnr1* KO mice than in *Sucnr1*$^{fl/fl}$ mice, concomitant with a significant increase in cortical thickness and bone perimeter around the midshaft (Figure 3A). The trabecular bone architecture of the same mice was unchanged (Figure 3B), but tibial length was significantly longer in Ad-*Sucnr1* KO mice (Figure 3C). Comparable numbers of osteoclasts per bone surface were observed between genotypes (Figure 3D), but hematoxylin/eosin (H&E) staining of tibiae sections revealed a significantly higher number of osteocytes per bone area in cortical bone of Ad-*Sucnr1* KO mice, together with a greater number of osteoblasts in bone surfaces of both cortical and trabecular bone (Figure 3E). Similar to adipocytes, osteoblasts derive from mesenchymal stem cells (MSCs)[38]. Analysis of the osteoblast differentiation potential of bone-marrow-MSCs failed to reveal significant differences between genotypes (Figure S3A). Changes to the bone phenotype were less evident in mice on HFD (Figure S3B and S3C), and the increase in bone volume, cortical thickness, trabecular number, and the number of osteocytes were not significant. Altogether, these findings point to a potential indirect effect of adipocyte-specific deletion of *Sucnr1* on postnatal growth and bone development, which might explain the initial body weight differences between genotypes.

Mice with conditional adipocyte deletion of *Sucnr1* have disturbances in leptin expression

Mice with global loss of *Sucnr1* on NCD have low fasting levels of some adipokines[3], suggesting a possible endocrine role for SUCNR1 in adipocytes. Given the metabolic phenotype of Ad-*Sucnr1* KO mice in terms of food intake and fat and bone mass, we investigated leptin as a master regulator of these biological processes. Strikingly, the circulating leptin response to refeeding was substantially weaker in global *Sucnr1* KO than in wild-type (WT) mice (Figure 4A). This was also evident in Ad-*Sucnr1* KO mice (Figure 4B). Additionally, the postnatal leptin surge that

occurs physiologically in mice[39] (10-day leptin=16.12±2.35 ng/mL vs 21-day leptin=2.83±0.57 ng/mL, *Sucnr1*$^{fl/fl}$ mice) was affected by *Sucnr1* deficiency, as Ad-*Sucnr1* KO mice showed a trend for a decrease in the 10-day leptin level (Figure 4C). Consistent with this, *Lep* gene expression in WAT (Figure 4D) and serum leptin levels (Figure 4E) were significantly lower in adult Ad-*Sucnr1* KO mice than in *Sucnr1*$^{fl/fl}$ mice, which might explain the hyperphagia in Ad-*Sucnr1* KO mice on NCD (Figure 1C). Furthermore, Ad-*Sucnr1* KO mice displayed a disturbance in the natural regulation of appetite-related neuropeptides during the fasting-feeding transition, particularly those associated with orexigenic signaling (*Npy* and *Agrp*) (Figure 4F). In line with this, fed-induced STAT3 phosphorylation (a surrogate marker of leptin signaling) was diminished in the hypothalamus of Ad-*Sucnr1* KO mice (Figure 4G, Figure S4A), which was not associated with changes in leptin sensitivity (Figure 4H and 4I).

Circulating levels of leptin are proportional to body fat mass[19,20]. No differences were observed in leptin levels between Ad-*Sucnr1* KO and control mice on HFD (*Sucnr1*$^{fl/fl}$=65.4±8.1 ng/mL *vs* Ad-*Sucnr1* KO=64.3±5.2 ng/mL), despite the trend for greater fat mass in the former (Figure 2C). Notably, the positive correlation between fat mass and leptin levels in *Sucnr1*$^{fl/fl}$ mice fed NCD or HFD (r=0.932, p=0.006; r=0.995, p=0.0004, respectively) was lost in Ad-*Sucnr1* KO mice (r=0.476, p=0.417; r=0.183, p=0.768, respectively), which supports our observations linking SUCNR1 to leptin.

We confirmed that the lower leptin levels found under standard dietary conditions were the consequence of *Sucnr1* deficiency and not an indirect effect of the lower fat mass in Ad-*Sucnr1* KO mice. Basal leptin release was lower in Ad-*Sucnr1* KO WAT *ex vivo* explants than in controls (Figure 4J). Of note, exogenous succinate enhanced *Lep* gene expression in *Sucnr1*$^{fl/fl}$ adipocytes but not in adipocytes from Ad-*Sucnr1* KO mice (Figure 4K). The expression of typical adipogenic markers (e.g., *Pparg*, *Fasn* and *Slc2a4*) was comparable between adipocytes from both genotypes (Figure 4L), indicating that the nonresponse of Ad-*Sucnr1* KO adipocytes was a consequence of *Sucnr1* deficiency, rather than a defect in differentiation. Finally, oral administration of succinate provoked a significant increase in plasma leptin levels in *Sucnr1*$^{fl/fl}$ mice but not in Ad-*Sucnr1* KO mice (Figure 4M), confirming a role for the succinate/SUCNR1 axis in leptin regulation.

To investigate whether the low leptin levels are related to the metabolically favorable phenotype of Ad-*Sucnr1* KO mice under NCD, we performed a 4-week leptin intervention. Leptin replacement therapy increased adipocyte size (Figure 4N) and impaired glucose tolerance (Figure 4O) in Ad-*Sucnr1* KO mice. This suggests that the low leptin levels observed in Ad-*Sucnr1* KO

mice on NCD, together with the induction of WAT browning (Figure 1I), are likely both associated with the reduction in adiposity of Ad-*Sucnr1* KO mice.

Succinate/SUCNR1 signaling controls leptin expression in an AMPK/JNK/C/EBP-α-dependent manner

To question how succinate/SUCNR1 signaling controls leptin expression, we first evaluated the effect of SUCNR1 activation on leptin expression in murine 3T3-L1 adipocytes. Similar to our findings in *Sucnr1*$^{fl/fl}$ adipocytes (Figure 4K), exposure to succinic acid significantly increased *Lep* expression in 3T3-L1 adipocytes (Figure 5A), an effect that was mimicked by the SUCNR1 agonist *cis*-epoxysuccinic acid (*c*ESA) (Figure 5B). We confirmed this in human adipocytes, finding also a positive effect of extracellular succinic acid on leptin release (Figure 5C). No significant upregulation of adiponectin gene expression was observed (Figure S5A). SUCNR1 engagement in adipocytes induced c-Jun N-terminal kinase (JNK) and p38 mitogen-activated protein kinase (MAPK) phosphorylation in a dose- and time-dependent manner (Figure 5D). Notably, we also found that SUCNR1 activation triggered AMP-activated protein kinase (AMPK) phosphorylation/activation at Thr172, which is concomitant with a blockade of activating Ser473 phosphorylation of AKT and its downstream target glycogen synthase kinase 3 (GSK-3)[40]. Accordingly, activation of AMPK with 5-aminoimidazole-4-carboxamide ribonucleotide (AICAR) induced leptin expression in 3T3-L1 adipocytes (Figure 5E), similar to the activation of SUCNR1 (Figure 5A). Of note, *c*ESA-induced AMPK activation was blunted in *ex vivo* WAT explants from Ad-*Sucnr1* KO mice (Figure 5F, Figure S4B). Treatment of 3T3-L1 cells with succinic acid increased insulin sensitivity (Figure 5G), which is in agreement with the beneficial effects reported for AMPK on glucose homeostasis[41]. To define the intracellular signaling pathways underlying leptin regulation by SUCNR1, we blocked these signaling cascades with specific chemical inhibitors. Inhibition of JNK (with SP600125) and AMPK (with compound C), but not p38 MAPK (with SB202190), completely blocked succinic acid-induced *Lep* expression (Figure 5H). These effects were not observed for adiponectin expression (Figure S5B). Additionally, inhibition of AMPK with compound C blocked JNK phosphorylation induced by *c*ESA (Figure 5I). By contrast, inhibition of JNK with SP600125 had no effect on the *c*ESA-mediated activation of AMPK (Figure 5I), suggesting that AMPK is upstream of JNK in the signaling cascade. Treatment of 3T3-L1 cells with *c*ESA also induced C/EBP-α phosphorylation (involved in leptin gene expression[42,43]), which was blocked by AMPK and JNK inhibitors (Figure 5I and 5J). Overall, these results suggest that succinate/SUCNR1 signaling controls leptin gene expression *via* the AMPK/JNK/C/EBP-α axis.

SUCNR1 activation regulates peripheral clock in adipose tissue

We profiled the transcription state of eWAT from Ad-*Sucnr1* KO and control mice. Gene set enrichment analysis indicated that the most significant change resulting from loss of *Sucnr1* was the circadian rhythm (Figure 6A). Differential gene expression analysis provided a deeper insight into the misalignment of the circadian rhythm (Figure 6B, 6C and Table S1). Of the 103 genes differentially expressed in eWAT of Ad-*Sucnr1* KO and control mice (65 upregulated and 38 downregulated; fold change >1.25, adjusted $p<0.05$; Table S1), 11 are key regulators of circadian rhythm. Ten of these genes were significantly upregulated in Ad-*Sucnr1* KO mice, whereas the core circadian gene encoding the brain and muscle aryl hydrocarbon receptor nuclear translocator-like protein 1 (*Bmal1*) was significantly downregulated.

Given that leptin secretion is controlled by the adipocyte circadian clock[44–46], we evaluated the effect of SUCNR1 activation on the expression of core clock genes using 3T3-L1 adipocytes (Figure 6D). Exposure to succinic acid significantly increased the positive circadian clock gene *Bmal1*, and downregulated the negative clock genes (period (*Per*) 1, *Per2*, *Per3*), and retinoic acid receptor-related orphan receptor alpha (*Rora*). Luciferase reporter analysis in SUCNR1-overexpressing human embryonic kidney (HEK) 293 cells transiently transfected with a BMAL-LUC reporter confirmed that activated SUCNR1 enhanced the transcription of the *BMAL1* promoter (Figure 6E). Similar to leptin, *Bmal1* expression was also induced by AMPK activation (Figure 6F). Pharmacological inhibition of AMPK (and JNK) blocked succinic acid regulation of clock gene expression (Figure 6G), comparable with their effects on *Lep* expression (Figure 5H). We confirmed at the protein level that BMAL1 upregulation induced by SUCNR1 activation was dependent on AMPK and JNK activation (Figure 6H). SUCNR1 activation also increases the presence of nuclear BMAL1 (total and Ser42-phosphorylated form), which is known to modulate *BMAL1* transcriptional activity[47] (Figure 6I). Notably, the upregulation of *Lep* expression by succinate in *ex vivo* WAT explants was blocked in those from mice with a heterozygous *Bmal1* deletion (Figure 6J), an effect that was not related to changes in *Sucnr1* expression (Figure 6K), or to differences in succinate-induced AMPK activation (Figure 6L, Figure S4C). By contrast, *Bmal1*-deficient WAT explants showed a blunted response to succinate-induced C/EBP/α phosphorylation, which is in agreement with previous results demonstrating that BMAL1/CLOCK stimulates C/EBP/α-mediated leptin transcription[44]. Overall, our data point to the succinate/SUCNR1 axis as a critical regulator of circadian clock in adipose tissue that impacts leptin expression.

Leptin regulation by succinate/SUCNR1 signaling is disturbed in obesity

A paradoxical hallmark of obesity is hyperleptinemia, which is sufficient to promote resistance to its anorexigenic effects[48]. We previously demonstrated that circulating succinate[10] and

SUCNR1 in adipocytes[34] is elevated in human obesity. In line with this, mature adipocytes differentiated from adipocyte precursors of subjects with obesity released more leptin in response to SUCNR1 activation than did adipocytes from lean counterparts (Figure 7A). To explore the link between leptin and the succinate/SUCNR1 axis in human obesity, we measured the circulating levels of leptin and succinate in a cohort of 56 subjects classified according to body mass index (BMI) (clinical and laboratory data are summarized in Table S2). As expected, circulating succinate and leptin levels were significantly higher in subjects with obesity (Table S2), and positively correlated with BMI in bivariate analysis (Figure S6). We then measured *LEP* and *SUCNR1* expression in scWAT and vWAT depots from the same subjects. In line with the obesity-related hyperleptinemia, *LEP* expression was significantly higher in scWAT of subjects with obesity, with a near significant increase in *SUCNR1* expression (Figure 7B). A trend towards increased *LEP* and *SUCNR1* expression was also observed in visceral fat depots (Figure 7C), which is consistent with our previous study[34]. Circulating leptin positively correlated with *LEP* expression in scWAT (Figure 7D), which in turn correlated with circulating succinate (Figure 7D). Bivariate analysis also revealed that *LEP* expression correlated with *SUCNR1* expression in both scWAT and vWAT (Figure 7D). Finally, obesity was associated with an overall increase in the expression of several core-clock genes, and this was particularly pronounced in vWAT (Figure 7E). Only *CLOCK* expression in scWAT positively correlated with circulating leptin (Figure 7F).

We next constructed multiple regression analysis models including the significant bivariate correlations for each dependent variable (Figure S6), adjusting for age and sex. The best model showed that the main predictors of circulating leptin were *LEP* expression in scWAT (b=2.261, beta=0.286, $p<0.05$), sex (b=17.841, beta=0.584, $p<0.001$) and BMI (b=0.831, beta=0.359, $p<0.05$) (Table S3). Notably, *SUCNR1* expression emerged as an independent factor associated with *LEP* expression in scWAT (b=0.434, beta=0.450, $p<0.01$) (Table S4) and vWAT (b=0.277, beta=0.470, $p<0.01$) (Table S5). These data show that obesity-associated hyperleptinemia is linked to elevated circulating levels of succinate and *SUCNR1* expression in adipose tissue, supporting the overactivation of this circuit in an obesity context.

DISCUSSION

We show that loss of succinate/SUCNR1 signaling in adipocytes inversely impacts WAT mass and glucose homeostasis according to nutritional status, a phenotype similar to that observed in global *Sucnr1* KO mice[3]. While previous studies have ascribed this phenotype to the anti-lipolytic effects of SUCNR1 and "unrestrained lipolysis"[3,31], our present analysis identifies a new additional function for succinate/SUCNR1 in adipocytes in regulating circadian clock and leptin expression, which also contributes to the regulation of energy homeostasis. Of note, we identify the precise contribution of succinate to the dichotomous effects of *Sucnr1* deficiency: the poor metabolic phenotype of Ad-*Sucnr1* KO mice during nutritional challenge is mostly contingent on the anti-lipolytic effect of SUCNR1, in agreement with a previous report[31], whereas its function as a regulator of leptin prevails in standard dietary states.

SUCNR1 is predominantly expressed in WAT and is highly abundant in purified adipocytes[3,4]. SUCNR1 has been suggested as a regulator of energy homeostasis through its participation in the breakdown of stored triglycerides in fat[4]. Consistent with an anti-lipolytic role, disruption of *Sucnr1* specifically in adipocytes leads to lower WAT mass. However, the decrease in adiposity was not reflected by ectopic triglyceride storage, but instead correlated with improved glucose tolerance, and a preference for carbohydrates as fuel[49,50]. Notably, neither global[3] nor adipocyte-specific KO mice present with elevated serum lipids, as observed in other models of unrepressed lipolysis[51–53]. Indeed, inhibition of lipolysis had no effect on fat mass or glucose tolerance, suggesting that it is not the main driver of the metabolically favorable phenotype in NCD. Rather, specific deletion of *Sucnr1* in adipocytes induced WAT browning, which is known to be associated with reduced weight gain and glucose tolerance[54,55]. The white-to-brown phenotypic switch is linked to the higher brown adipocyte differentiation capacity of adipocyte precursors, likely favored by the local accumulation of succinate, which has been recently identified as a thermogenic activator[14] and browning agent[36].

These aforementioned mechanisms seem not to operate in response to overnutrition, where the impact of global loss of *Sucnr1* is more complex and contentious[3,33]. We found that HFD-feeding of Ad-*Sucnr1* KO mice increased fat deposition in liver, which was accompanied by glucose intolerance, as previously observed in global *Sucnr1* KO mice[3]. A similar study did not observe the same phenotype[33], most likely because of the different mouse models or the different diets/periods used, stressing the need for tissue-specific KO models to precisely capture the effects of *Sucnr1* deficiency in individual cell types. Our study confirms that the function of SUCNR1 as an anti-lipolytic effector in adipocytes is dominant in the context of overnutrition,

which is in line with a recent report demonstrating that modulation of succinate export from the mitochondria mimics the metabolic phenotype of our model in an obesity setting[31].

Beyond its role as a regulator of lipolysis, adipocyte-specific deletion of *Sucnr1* revealed an unexpected phenotype in terms of bone mass, which might partly underlie the higher body weight of Ad-*Sucnr1* KO mice. The inverse relationship between WAT and bone mass has been observed in other models of gene-specific deletion in adipocytes[56–58]. Perturbations in MSCs commonly cause this phenotype[56–59], but this does not seem to be the case in our model. Adipocyte deletion of *Sucnr1* results in lower levels of circulating leptin, which is a relevant factor in the regulation of bone mass[60,61]. While *in vitro* research suggests leptin as a positive regulator of chondrocytes and osteoblasts[62,63], many other experimental and clinical studies indicate that it is a major negative regulator of bone mass accrual by a central hypothalamic mechanism, and independently of fat mass[64,65]. Indeed, obesity-related hyperleptinemia has been linked to decreased bone mass, even in the presence of leptin resistance[66–68]. We observed hypoleptinemia and an impaired leptin response to feeding in Ad-*Sucnr1* KO mice, which was mirrored by a disturbance in the hypothalamic response during the fasting-to-fed transition. Therefore, the cortical phenotype found in young Ad-*Sucnr1* KO mice supports leptin as a negative regulator of bone mass at the central level, which could be particularly relevant during postnatal bone development.

Our data point to succinate as a hormone-like metabolite with a key role in regulating leptin production, which is a novel physiological and molecular mechanism. SUCNR1 also emerges as a novel regulator of circadian clock in adipose tissue, which is consistent with data from Kettner and colleagues who show that leptin expression, which exhibits diurnal variation in both human and rodents[69,70], is under the control of an adipose tissue peripheral clock in a CLOCK-BMAL1-C/EPB/α dependent manner[44]. *Sucnr1* deletion disturbs the expression profile of core-clock genes, in accordance with a disruption in feeding behavior in mice fed NCD or HFD. While no data exists on circadian rhythmicity of circulating succinate, it is regulated by food intake[15,71], and succinate levels in saliva are under circadian control[72]. Because peripheral tissues such as adipose tissue respond to changes in food cues and nutrient sensors independent of the central clock to regulate nutrient uptake and metabolism[73–75], it is conceivable that succinate operates as an internal physiological signal to influence the circadian period in addition to regulating lipid metabolism[3,31]. Published circadian transcriptome datasets of adipose tissue have yielded conflicting results[76–79], likely due to species-specific differences and operational difficulties. Interestingly, the study of circadian transcriptome in human WAT under constant, routine protocols predicts circadian variation in the tricarboxylic acid cycle[76], and analysis of *Sucnr1* gene expression profile in CircadiOmics[80] reveals a circadian profile in primates, particularly in

baboon. Our study identifies a novel transduction pathway by which succinate *via* a SUCNR1-AMPK-JNK-dependent mechanism controls BMAL1-C/EBP/α-mediated regulation of leptin.

It is possible that peripheral SUCNR1 is activated in healthy tissues to regulate metabolic homeostasis in response to food ingestion[15], and changes in circulating succinate after feeding thus emerge as a novel regulator of leptin expression. MAPK signaling pathways have been previously shown to mediate some SUCNR1-dependent effects[81]. Unexpectedly, we found that SUCNR1 engagement in adipocytes also activates AMPK, a master regulator of energy metabolism that functions to rewire metabolism by reducing anabolic processes and increasing catabolism[82]. Indeed, fasting[83,84] and exercise[85] activate AMPK in adipose tissue. Nonetheless, and similar to what occurs in skeletal muscle[86], AMPK activation in adipocytes enhances basal glucose uptake[87,88], a process that is stimulated after food ingestion. Moreover, similar to insulin and succinate, AMPK activation in adipocytes inhibits lipolysis[89,90], which suggests that its function in adipose tissue goes beyond activating catabolic processes. Indeed, AICAR, a direct activator of AMPK, up-regulates the expression of adiponectin in human adipose tissue[91,92], and both adiponectin[92,93] and leptin[94] can activate AMPK in adipocytes. Remarkably, there is also evidence that some of the metabolic effects of AMPK might be mediated through the regulation of circadian clock[95]. Our results show an increase of BMAL1 expression by AMPK activation, which is in agreement with previous studies reporting that AMPK promotes BMAL1 expression by inducing the degradation of PER2[96] and destabilization of the core clock protein CRY1[97]. Our evidence for SUCNR1 and AMPK as direct regulators of circadian clock and leptin in adipocyte physiology is supported by human data showing that *SUCNR1* expression is an important determinant of leptin levels in adipose tissue.

Beyond its physiological relevance, our study in the context of obesity demonstrates that disturbances in the succinate/SUCNR1 axis are linked to obesity-related hyperleptinemia. We and others recently demonstrated that succinate is involved in the natural resolution of inflammation[34,98], yet obesity is linked to perturbations in this system associated with high levels of circulating succinate but reduced expression of *Sucnr1* in adipose-tissue resident macrophages[34]. This would represent a novel mechanism behind the inability of people with obesity to resolve uncontrolled inflammation. Conversely, “obese” adipocytes show higher expression of *SUCNR1*, and are more sensitive to succinate-induced leptin release. Thus, we propose that obesity is associated with hyperactivation of succinate/SUCNR1 signaling in adipocytes, which increases leptin production.

Overall, our study contributes towards the development of a holistic perspective of the succinate/SUCNR1 axis as part of the metabolite-sensing machinery that allows adipocytes to

coordinate metabolic responses in response to nutrient intake. Thus, changes in circulating succinate during the fasted-to-fed transition might serve a physiological function in adipose tissue by regulating not only lipolysis, but also leptin *via* SUCNR1. Dysregulation of this system in obesity emerges as a novel causal mechanism of obesity-related hyperleptinemia. Further research is needed to provide a complete picture of succinate as a signal transducer of physiological functions, and a potential regulator of circadian clock. The possibility of SUCNR1 as a pharmacological target will require exhaustive investigation to understand the mechanics of the succinate/SUCNR1 axis in both health and disease.

LIMITATIONS OF THE STUDY

Our study has some limitations. Experiments on animals were performed in the spirit of the 3Rs. Reduction strategy was used even the small samples sizes used for some experiments limited our ability to detect statistically significant differences for certain parameters, but provide sufficient data to answer the research question. Also, only male mice were used as our initial experiments confirmed a similar phenotype in both sexes. BMAL1 activation by SUCNR1 was confirmed in a heterologous host (human SUCNR1-transfected HEK293 cells) rather than mature adipocytes (the most suitable cell model) due to their low transfection efficiency. Finally, we acknowledge that to strengthen the translational relevance of our findings, the expression of clock genes in the human cohort would benefit from a temporal analysis to provide a more accurate perspective of the circadian dynamics in obesity.

ACKNOWLEDGEMENTS

This study was supported by grants from the Spanish Ministry of Science and Innovation (MCIN) (SAF2015-65019-R and RTI2018-093919-B-100 to S.F.-V., PI20/00095 to V.C.-M., and PI20/00338 to J.V.), co-financed by the European Regional Development Fund (ERDF). This research was also supported by PID2020-119030RJ-I00 (to L.Cedó), PID2020-117640RB-I00 (to M.V.), and PID2020-117278GB-I00 (to F.V.) from MCIN/AEI/10.13039/501100011033/. The project that gave rise to these results received funding from "La Caixa" Foundation under the grant agreement LCF/PR/HR20/52400013 (to S.F.-V.). N.V. is the recipient of grants "Ajuts per a projectes de recerca clínica de l'Hospital Universitari de Bellvitge (2011-PR143/11)" and of the projects PI11/01960, PI14/01997, and PI17/01556 funded by the Instituto de Salud Carlos III and co-funded by "ERDF, A way to build Europe". T.V.-C. is a recipient of an FPI fellowship (PRE2019-090360), and V.C.-M. acknowledges support from the Ramón y Cajal program (RYC2019-02649-I), both from MCIN/AEI/10.13039/501100011033/ and "European Social Fund (ESF) Investing in your future". M.R.-D.-D. is recipient of a Martí-Franquès Research Grant Programme (2021PMF-PIPF-2) from Universitat Rovira i Virgili. C.P-L. is recipient of an FPU fellowship from the Spanish Ministry of Education. J.S.-B. is a recipient of a predoctoral contract for training in health research from the Instituto de Salud Carlos III, co-financed by the ESF (PFIS FI18/00151). S.F.-V. acknowledges support from the Miguel Servet tenue-track program (CP10/00438 and CPII16/00008) from the Fondo de Investigación Sanitaria, co-financed by the ERDF. The Spanish Biomedical Research Center in Diabetes and Associated Metabilic Disorders (CIBERDEM) (CB07708/0012) is an initiative or the Instituto de Salud Carlos III. We thank the Genomics Unit at the CRG for assistance with the sequencing, and the Biostatistics/Bioinformatics facility (IRB, Barcelona, Spain) for assistance with data analysis. We particularly acknowledge the patients and the BioBank IISPV (PT17/0015/0029) integrated in the Spanish National Biobanks Network (registration number #C.0003609) for their collaboration. We thank G. Sabio (CNIC, Spain) for kindly providing the transgenic mice expressing Cre recombinase driven by the adipocyte-specific *Adipoq* promoter, and Kristin Mahan (University of Texas, USA) and Shin Yamazaki (UT Southwestern Medical Center, USA) for kindly providing the pGL3 BMAL-LUC construct. We thank Marc Claret (IDIBAPS, Barcelona), Sara Ramírez (IDIBAPS, Barcelona), and Aleix Ribas-Latre (University of Leipzig, Germany) for their scientific advice in some aspects of the research, and Kenneth McCreath for helpful comments on the manuscript.

AUTHOR CONTRIBUTION

Conceptualization, T.V.-C., L.Cedó, J.V., and S.F.-V.; Methodology, T.V.-C., L, Cedó, A.M., M.-M.R.-P., C.N.-R., E.M.-M., M.R.-D.-D., N.K., J.S.-B., and R.B.; Formal Analysis, T.V., L.Cedó, A.M., V.C.-M., and J.B.; Investigation, T.V.-C., L.Cedó, A.M., M.M., C.P.-L., and J.C.E.-G.; Resources, L.Caubet, J.M.F.-R., and N.V.; Writing – Original Draft, T.V.-C., L.Cedó, A.M., J.V., and S.F.-V.; Writing – Review & Editing, M.V., F.V., J.V., and S.F.-V.; Supervision, J.V. and S.F.-V.; Funding Acquisition, M.V., F.V., J.V., and S.F.-V.

DECLARATION OF INTERESTS

The authors declare no competing interests.

INCLUSION AND DIVERSITY

We worked to ensure gender balance in the recruitment of human subjects. We worked to ensure that the study questionnaires were prepared in an inclusive way. While citing references scientifically relevant for this work, we also actively worked to promote gender balance in our reference list.

FIGURE TITLES AND LEGENDS

Figure 1. Conditional adipocyte deletion of *Sucnr1* reduces adipose mass and improves systemic metabolic health. (A) Body weight progression in Ad-*Sucnr1* KO and *Sucnr1*$^{fl/fl}$ mice fed NCD for 29 weeks (n=14 *Sucnr1*$^{fl/fl}$; n=12 Ad-*Sucnr1* KO). **(B)** Changes in body weight (n=6 mice/group). **(C)** Food intake during light and dark hours (left) and regression-based plot of food intake with body weight as a covariate (right) (genotype p =0.034 in dark) (n=6/group). **(D)** RER (left: time-course; and right: average/mouse) at week 12 of life (p=0.003) (n=6/group). **(E)** qMRI quantification of scWAT, vWAT, and total WAT mass, and representative qMRI images of fat (n=8 *Sucnr1*$^{fl/fl}$; n=6 Ad-*Sucnr1* KO) at week 12 of life. **(F)** Representative H&E-stained images of iWAT and eWAT, and quantification of adipocyte area. **(G)** GTT and its respective area under the curve (AUC) at week 25 of life (n=6 mice/group). **(H)** ITT and its respective AUC at week 25 of life (n=6 mice/group). **(I)** Representative images of UCP1 immunohistochemistry, and *Ucp1* relative gene expression in iWAT (n=5/group). **(J)** Representative Oil-red O-stained images of mouse adipose tissue stem cells (mASCs) undifferentiated and differentiated to brown adipocytes, and quantification of differentiation-induced lipid accumulation (n=6 *Sucnr1*$^{fl/fl}$; n=9 Ad-*Sucnr1* KO). **(K)** Fold change of *Ucp1* and *Cidea* expression in mASCs differentiated to brown adipocytes (n=6 *Sucnr1*$^{fl/fl}$; n=4 Ad-*Sucnr1* KO). **(L)** *Sucnr1* expression in mASCs (n=5 *Sucnr1*$^{fl/fl}$; n=3 Ad-*Sucnr1* KO). **(M)** Succinate accumulation in eWAT explants (n=7 *Sucnr1*$^{fl/fl}$; n=5 Ad-*Sucnr1* KO). Data are presented as box and whiskers plots showing median, first and third quartiles and maximum and minimum values; or as mean±SEM; *p<0.05, **p<0.01; ***p<0.001 (Unpaired t-test or Mann-Whitney test in box and whiskers plots, two-way ANOVA in **A**, **G**, and **H**, one-way ANOVA in **C** and **D**).

Figure 2. Mice with conditional adipocyte deletion of *Sucnr1* develop hepatic steatosis and glucose intolerance on high-fat diet. (A) Body weight progression and **(B)** body weight gain in Ad-*Sucnr1* KO and *Sucnr1*$^{fl/fl}$ mice fed HFD for 12 weeks, starting at 8 weeks of age (n=11 *Sucnr1*$^{fl/fl}$; n=4 Ad-*Sucnr1* KO). **(C)** qMRI quantification of scWAT, vWAT, and total WAT mass, and representative qMRI images of fat after 12 weeks of HFD feeding (n=5/group). **(D)** EE (left) and regression-based plot of EE with body weight as covariate (right) (weight p =0.034 and genotype p=0.437); **(E)** food intake during light and dark hours (left) and regression-based plot of food intake with body weight as a covariate (right) (genotype p=0.015 in light); and **(F)** RER (left: time-course; and right: average/mouse) (p=0.048) after 12 weeks of HFD feeding (n=5/group). **(G)** GTT and its respective AUC after 10 weeks of HFD feeding (n=5/group). **(H)** ITT and its respective AUC after 8 weeks of HFD feeding (n=5/group). **(I)** Representative H&E-stained images of iWAT, eWAT and liver. **(J)** Circulating levels of triglycerides and non-esterified fatty acids (n=8 *Sucnr1*$^{fl/fl}$ and n=6 Ad-*Sucnr1* KO fed NCD; n=5 *Sucnr1*$^{fl/fl}$ and n=4

Ad-*Sucnr1* KO fed HFD). **(K)** Liver H&E staining and **(L)** GTT in Ad-*Sucnr1* KO mice fed HFD for 8 weeks and treated with ATGLi or vehicle (corn oil) for 2 weeks (n=3 vehicle- and n=4 ATGLi-treated mice). Data are presented as box and whiskers plots showing median, first and third quartiles and maximum and minimum values, or as mean±SEM; *p<0.05; **p<0.01 (Unpaired t-test or Mann-Whitney test in bar graphs; two-way ANOVA in **A**, **G**, **H**, and **L**; ANCOVA in **D**; and one-way ANOVA in **E** and **F**).

Figure 3. Mice with conditional adipocyte deletion of *Sucnr1* develop a bone mass phenotype. Microcomputed tomography analysis and representative images of **(A)** cortical and **(B)** trabecular tibia (n=7–8 *Sucnr1*$^{fl/fl}$ and n=6 Ad-*Sucnr1* KO). **(C)** Tibia length (n=8 *Sucnr1*$^{fl/fl}$ and n=6 Ad-*Sucnr1* KO). **(D)** Quantification of the number of osteoclasts (Ocl) and representative images of TRAP staining (n=4/group). **(E)** Quantification of the number of osteoblasts (OB) and osteocytes (Ocy), and representative images of H&E staining (n=4/group). Data are presented as box and whisker plots showing median, first and third quartiles and maximum and minimum values; *p<0.05, **p<0.01; ***p<0.001 (Unpaired t-test or Mann-Whitney test).

Figure 4. Mice with conditional adipocyte deletion of *Sucnr1* have disturbances in leptin expression. Feeding-induced circulating leptin response in **(A)** WT (n=5) and global *Sucnr1* KO mice (n=4); and in **(B)** Ad-*Sucnr1* KO (n=6) and *Sucnr1*$^{fl/fl}$ (n=5) mice. **(C)** Circulating leptin increase at 10 days normalized to 21-day leptin levels (n=5 *Sucnr1*$^{fl/fl}$ and n=6 Ad-*Sucnr1* KO). **(D)** *Lep* expression in iWAT and retroperitoneal WAT (rWAT) (n=5 mice/group). **(E)** Circulating levels of leptin in 29-week old mice (n=5 mice/group). **(F)** *Npy* and *Agrp* expression in hypothalamus in fasted and refed states (n=4 mice/group). **(G and H)** Representative immunoblot images of p-STAT3 in hypothalamus, and densitometry analysis from Ad-*Sucnr1* KO and *Sucnr1*$^{fl/fl}$ mice **(G)** in fasted and refed states (n=6); or **(H)** treated with leptin (n=4). β-ACTIN was used as a loading control. **(I)** Food intake (n=4/group) and body weight change (n=4 *Sucnr1*$^{fl/fl}$ and n=5 Ad-*Sucnr1* KO) induced by 4-day leptin treatment. **(J)** Leptin secretion by iWAT and rWAT explants (n=11 *Sucnr1*$^{fl/fl}$ and n=7–9 Ad-*Sucnr1* KO). **(K)** Fold change of *Lep* expression in primary adipocytes isolated from iWAT and eWAT and treated with succinic acid (n=3–5 animals/group). **(L)** *Pparg*, *Fasn*, and *Slc2a4* expression in mature adipocytes isolated from iWAT, and eWAT (n=6–7 mice/group). **(M)** Circulating leptin levels after an oral administration of sodium succinate (n=6 *Sucnr1*$^{fl/fl}$ and n=4 Ad-*Sucnr1* KO). **(N)** Representative H&E staining of WAT, and quantification of adipocyte area; and **(O)** GTT in Ad-*Sucnr1* KO mice treated with leptin or vehicle for 4 weeks (n=4 vehicle- and n=5 leptin-treated mice). Data are presented as box and whiskers plots showing median, first and third quartiles and maximum and minimum values, or as mean±SEM; *p<0.05; **p<0.01; ***p<0.001 (Unpaired t-test or Mann-Whitney test in bar graphs and two-way ANOVA in time-course graphs).

Figure 5. Succinate/SUCNR1 signaling controls leptin expression in an AMPK/JNK/C/EBP-α-dependent manner. *Lep* expression in differentiated 3T3.L1 cells treated with **(A)** succinic acid or **(B)** *c*ESA. **(C)** Leptin gene expression and secretion in adipocytes differentiated from human ASCs (hASCs) and treated with succinic acid. **(D)** Representative immunoblot images of phosphorylated kinases in 3T3-L1 adipocytes treated with *c*ESA, and densitometry analysis of *c*ESA (100 μM)-induced phosphorylation. β-ACTIN was used as a loading control. **(E)** *Lep* expression in differentiated 3T3-L1 cells treated with AICAR (n=5–6). **(F)** Representative immunoblot images and densitometry analysis of p-AMPK in WAT explants from Ad-*Sucnr1* KO and *Sucnr1*$^{fl/fl}$ mice treated with *c*ESA. Total AMPK was used as a loading control. **(G)** Representative immunoblot images of phosphorylated kinases in 3T3.L1 adipocytes treated with succinic acid and insulin. Densitometry analysis normalized to the control treated with insulin. β-ACTIN was used as a loading control. **(H)** *Lep* expression in differentiated 3T3-L1 cells treated with inhibitors and succinic acid (n=6–9). **(I** and **J)** Representative immunoblot images of phosphorylated kinases in 3T3-L1 adipocytes treated with compound C or SP600125, and *c*ESA; and densitometry analysis. β-ACTIN was used as a loading control. Data are presented as box and whisker plots showing median, first and third quartiles and maximum and minimum values, or as mean±SEM. Unless indicated, n=2–4 independent samples. *p<0.05; **p<0.01; ***p<0,001 *vs* time 0 or control (one-way or two-way ANOVA when comparing more than two groups *vs* control; or unpaired *t*-test or Mann-Whitney test when comparing two groups).

Figure 6. SUCNR1 activation regulates peripheral clock in adipose tissue. (A–C) RNAseq gene expression of eWAT from *Sucnr1*$^{fl/fl}$ and Ad-*Sucnr1* KO mice (n=5/group). **(A)** Bar plots showing normalized enrichment scores (nes) annotated according to the Kyoto Encyclopedia of Genes and Genomes (KEGG) pathways, distinguishing between downregulated and upregulated pathways (filtered by gene sets with p<0.05). **(B)** Volcano plot for differential gene expression. *P*-values were adjusted for multiple comparisons using the Benjamini-Hochberg procedure. Circadian clock genes with adjusted p<0.05 are labeled. **(C)** Heatmap showing relative expression levels for genes in the circadian rhythm pathway annotated according to the KEGG pathway and manually annotated (at the bottom). *P*-values were adjusted for multiple comparisons using the Benjamini-Hochberg procedure. **(D)** Relative expression of circadian rhythm genes in differentiated 3T3-L1 cells treated with succinic acid (n=2–6). **(E)** Luciferase assay showing expression from BMAL1-LUC in SUCNR1-overexpressing HEK 293 cells transfected with the BMAL1-LUC reporter and treated with *c*ESA and SR1078. **(F)** *Bmal1* expression in differentiated 3T3-L1 cells treated with AICAR (n=2–3). **(G)** Succinic acid and compound C (CC) or SP600125 (SP)-induced relative expression of circadian rhythm genes in differentiated 3T3-L1 cells (n=4). **(H)** Representative immunoblot images of BMAL1 in 3T3-L1 cells treated

with *c*ESA ± CC or SP; and densitometry analysis. β-ACTIN was used as a loading control (n=2–4). (**I)** Representative immunoblot images of p-BMAL1 and BMAL1 in the nuclear fraction of 3T3-L1 cells after treatment with *c*ESA; and densitometry analysis. LAMIN A was used as a loading control (n=3–9). **(J)** *Lep* expression in iWAT explants from *Bmal1* KO and WT mice treated with succinic acid (n=3–4). **(K)** Basal gene expression in iWAT explants from *Bmal1* KO and WT mice (n=4). **(L)** Representative immunoblot images of phosphorylated kinases in iWAT explants from WT and *Bmal1* KO mice treated with succinic acid; and densitometry analysis. β-ACTIN was used as a loading control (n=4). Data are presented as box and whiskers plots showing median, first and third quartiles and maximum and minimum values, or as mean±SEM; **p*<0.05; ***p*<0.01; and ****p*<0.001 *vs* time 0 or control; and ‡ *p*<0.05; ‡‡ *p*<0.01; and ‡‡‡ *p*<0.001 *vs* succinic acid-treated cells in **F** (one-way ANOVA when comparing more than two groups *vs* time 0 or control; or unpaired *t*-test when comparing two groups).

Figure 7. Leptin regulation by succinate/SUCNR1 signaling is disturbed in obesity. (A) Leptin secretion in adipocytes differentiated from lean or obese hASCs treated with *c*ESA (n=4). **(B)** *LEP* and *SUCNR1* expression in scWAT (n=12 lean and n=20 obese subjects). **(C)** *LEP* and *SUCNR1* expression in vWAT (n=9 lean and n=24 obese subjects). **(D)** Correlation between circulating leptin or succinate and scWAT *LEP* expression, and between *SUCNR1* and *LEP* expression in scWAT and vWAT. **(E)** Relative gene expression of clock genes in scWAT and vWAT (n=8 lean and n=19 obese subjects). **(F)** Correlation between circulating leptin and *CLOCK* expression in scWAT. **p*<0.05; ***p*<0.01; ****p*<0,001 (two-way ANOVA *vs* t = 0 in **A**; or unpaired *t*-test or Mann-Whitney test for violin graphs). For **D** and **F** nonparametric Spearman's correlation analysis was used.

STAR METHODS

RESOURCE AVAILABILITY

Lead contact

Further information and requests for resources and reagents should be directed to and will be fulfilled by the Lead Contact: Sonia Fernández-Veledo (sonia.fernandez@iispv.cat).

Materials availability

Mouse lines generated in this study are available from the lead contact upon request.

Data and code availability

- RNAseq data have been deposited in GEO and are publicly available as of the date of publication. Accession numbers are listed in the key resources table.
- This study did not generate new code.
- Any additional information required to reanalyze the data reported in this paper is available from the lead contact upon request.
- Data S1 refers to unprocessed data underlying the display items in manuscript, related to Figures 1–7 and S1–S4.

EXPERIMENTAL MODEL AND SUBJECT DETAILS

Human cohorts

Subjects were recruited at the University Hospital Joan XXIII (Tarragona, Spain) and Hospital de Santa Tecla (Tarragona, Spain). All participants gave their informed consent and the study was reviewed and approved by the ethics and research committees of the respective hospitals (references CEIm 177/2018 approved on the 29th of November 2018 and CEIm 41p/2015 approved on the 31st of August 2015), in accordance with the tenets of the Declaration of Helsinki. Plasma, scWAT and vWAT were obtained from age- and gender-matched human donors undergoing non-acute surgical interventions, such as hernia or cholecystectomy, in a scheduled routine surgery. Donors were classified according to their BMI as lean or obese, following World Health Organization criteria[99] (lean BMI $\leq$25 kg/m^2 and obese BMI $\geq$30 kg/m^2). Anthropometric and biochemical variables from the cohort are detailed in Table S2.

Mouse lines

Adipocyte cell-specific *Sucnr1* knockout mice (Ad-*Sucnr1* KO) were generated by breeding *Adipoq*-Cre mice (kindly provided by G. Sabio, CNIC, Madrid, Spain) with *Sucnr1*$^{fl/fl}$ mice[34]. Cre-

negative *Sucnr1*$^{fl/fl}$ littermates were used as controls. Mice were genotyped by PCR; genotyping of *Sucnr1*$^{fl/fl}$ mice resulted in a 450-bp product for the *loxP*-targeted allele and a 700-bp product for the *Adipoq*-Cre allele. All genotypes were generated on a pure C57BL/6 background. Mice were housed at the Faculty of Medicine and Health Science animal facility of Universitat Rovira i Virgili, under controlled conditions of 12-h light/dark cycles at 22ºC and *ad libitum* access to NCD (3.1% fat; SAFE diets, A04) or HFD (60% fat; Research diets, D12492), unless specified, beginning at 8 weeks of age until sacrifice. Male mice were weighed weekly. At the end of the study, animals were fasted overnight, killed by cervical dislocation, and blood and tissues were collected and immediately frozen. Plasma was obtained from global *Sucnr1* KO[3] and wild-type mice (C57BL/6; Charles River, Barcelona, Spain) used as controls, as well as from Ad-*Sucnr1* KO and *Sucnr1*$^{fl/fl}$ mice, after an overnight fast ± a 3-h refed. Adipose tissue was collected from 10–12-week-old male B6.129-*Arntl*^{tm1Bra}/J heterozygous knockout mice (#009100; RRID: IMSR_JAX:009100; *Bmal1* KO) purchased from The Jackson Laboratory (Bar Harbor, ME) and C57BL/6J wild-type mice were used as controls. The *Bmal1* expression levels were confirmed by qPCR in liver: 0.55±0.03 in *Bmal1* KO *vs* 1.00±0.11 in WT, p=0.002; and in rWAT: 0.65±0.03 in *Bmal1* KO *vs* 1.00±0.09 in WT, p=0.005. All animal studies were supervised and approved by the Universitat Rovira i Virgili Animal Welfare and Governmental Ethics Committee (reference 10970). All animal procedures conformed to European Union Directive 86/609/EEC and recommendation 2007/526/EC regarding the protection of animals used for experimental and other scientific purposes, enacted under Spanish law 1201/2005.

Mouse adipose tissue explants

Mouse WAT from at least three mice was freshly isolated and cleaned with phosphate buffered-saline (PBS; Hyclone, GE Healthcare Life Sciences, Logan, UT) containing 1% antibiotic/antimycotic solution (Hyclone) and pooled. For leptin secretion analysis, tissues (0.2 g) were transferred into 1 mL of DMEM/F12 (Gibco, Life Technologies Limited, Paisley, UK) for 24 h at 37ºC and 5% CO_2. Supernatants were then collected and stored at -20 ºC for further analysis. For western blot experiments, tissues (0.8 g) were cultured in 24-well plates with Krebs Ringer Bicarbonate HEPES (KRBH) buffer containing 120 mM NaCl, 5 mM KCl, 2 mM $CaCl_2$, 1 mM $MgCl_2$, 25 mM $NaHCO_3$, and 5.5 mM HEPES, and supplemented with 0.1% bovine serum albumin (BSA, Sigma-Aldrich, St Louis, MO) for 2 h, and treated with 100 µM *c*ESA (TCI chemicals, Tokyo, Japan) or 400 µM succinic acid (Sigma-Aldrich) for 10 min. For gene expression studies, tissues (0.8g) were cultured in 24-well plates with KRBH buffer supplemented with 0.1% BSA for 2 h and treated with 400 µM succinic acid for 6 h.

Primary mASCs and mature adipocytes

WAT was collected from Ad-*Sucnr1* KO and *Sucnr1*$^{fl/fl}$ mice, weighed, and pooled according to WAT localization and genotype. Tissues were cut into small pieces, extensively washed with PBS to remove debris, and treated with 0.2% collagenase (Sigma-Aldrich) in PBS and 1% BSA for 1 h at 37°C with gentle agitation. Digested samples were centrifuged at 300 g for 10 min to separate adipocytes from the stromal vascular fraction (SVF). Mature adipocytes were carefully removed from the upper part of the solution and centrifuged at 300 g for 5 min. Adipocytes were then cultured in 12-well plates with DMEM/F12 supplemented with 10% fetal bovine serum (FBS, Hyclone) for 24 h at 37ºC and 5% CO_2, and treated with 400 µM succinic acid for 6 h. The cell pellet containing the SVF was re-suspended in DMEM/F12 supplemented with 10% FBS and 1% antibiotic/antimycotic solution. Mouse ASCs were incubated at 37°C and 5% CO_2 and the medium was replaced 24 h after seeding to remove non-adherent cells. All experiments were performed in cells at passage 3.

Primary mouse BM-MSCs

Tibias and femurs from mice were dissected and cleaned with PBS. Bones were cut to allow flushing of bone-marrow contents using a 20-G needle attached to a syringe, and the pellet was cultured in DMEM-High Glucose medium (Hyclone) supplemented with 15% FBS and 1% antibiotic/antimycotic solution in a humidified cell culture incubator at 37°C with 5% CO_2. Non-adherent cells were removed after 24 h with subsequent media changes every 2–3 days until BM-MSCs reached confluence.

Primary hASCs

Human ASCs were isolated as described[100] from scWAT biopsies of lean and obese donors, which included 4 females (n=2 lean, BMI 20.3±0.7 kg/m^2; n=2 obese, BMI 32.9±0.7 kg/m^2). Briefly, adipose tissue was washed with PBS and then treated with 0.1% collagenase in PBS + 1% BSA for 1 h at 37°C with gentle agitation. Digested samples were centrifuged at 300 g at 4°C for 5 min to separate the SVF. The SVF was resuspended and cultured in DMEM/F12 supplemented with 10% FBS and 1% antibiotic/antimycotic solution, and frozen. Cells were stored in the IISPV BioBank (PT17/0015/0029) registered at the National Register of Biobanks (registration number #C.0003609). Differentiation of hASCs to mature white adipocytes was performed following a published protocol[101]. In brief, differentiation induction medium was used for confluent hASCs, containing DMEM/F12, 10% FBS, 1% antibiotic/antimycotic solution, DMEM-High Glucose, dexamethasone (1 µM), biotin (33 µM), calcium pantothenate (17 µM), 3-isobutyl-1-methylxanthine (IBMX; 500 µM), insulin (100 nM), and rosiglitazone (5 µM) (all from Sigma-Aldrich). After 4 days, the medium was changed every two days to supplemented DMEM/F12-DMEM-High Glucose medium only containing dexamethasone, biotin, and calcium pantothenate

until day 14 of differentiation. Once differentiated, cells were serum deprived for 2 h with FBS-free medium containing 0.2% BSA, and treated with 400 µM succinic acid or 100 µM *c*ESA.

3T3-L1 cell line

Murine embryonic 3T3-L1 preadipose cells (CL-173™; RRID: CVCL-0123; ATCC, Manassas, VA) were cultured in DMEM-High Glucose medium supplemented with 10% FBS and 1% antibiotic/antimycotic solution in a humidified cell culture incubator at 37°C with 5% CO_2. Confluent cultures were treated for 2 days in the same medium containing the differentiation inducers 0.25 µM dexamethasone, 0.5 mM IBMX, 5 µg/mL insulin, and 1 µM rosiglitazone. Cells were then cultured for 2 days in growth medium supplemented with 5 µg/mL insulin and 1 µM rosiglitazone, and then in growth medium alone for the subsequent days. At day 9–10 of differentiation, cells were rested for 2 h in FBS-free medium containing 0.2% BSA and then treated with succinic acid, *c*ESA, or 5-aminoimidazole-4-carboxamide ribonucleotide (AICAR; Sigma-Aldrich). In studies using phosphatase inhibitors, cells were pre-treated for 30 min with SP600125 (MedChemExpress, Monmouth Junction, NJ), SB202190 (MedChemExpress) or compound C (Calbiochem, San Diego, CA).

HEK 293 cell line

Human embryonic kidney (HEK) 293 cells were obtained from ATCC (CRL-1573™; RRID: CVCL_0045). Cells were cultured in DMEM-High Glucose supplemented with 10% FBS and 1% antibiotics/antimycotics solution.

METHOD DETAILS

Indirect calorimetry

Indirect calorimetry was performed as described[102] using a 16-chamber TSE Phenomaster monitoring system (TSE Systems GmbH, Bad Homburg, Germany). Individually caged mice were acclimatized in the measuring room for three days before the onset of experiments. Oxygen consumption and CO_2 production were directly measured over a period of 48 to 72 h. From these data, the RER and EE were calculated according to the formula $RER = V_{CO2}/V_{O2}$; $EE = (3.185 + 1.232 * RER) * V_{O2}$.

Locomotor activity and food intake

Locomotor activity and food intake were monitored during the indirect calorimetry experiments. Horizontal locomotor activity of mice moving freely in their cages was continuously registered using an infrared photocell beam grid. Food and water intake were automatically monitored using built-in sensors located in each cage, and were available *ad libitum* unless stated otherwise.

Quantitative Magnetic Resonance Imaging

Fat mass. The relative amount of fat in each animal was calculated using qMRI. Mice were anaesthetized with 1.5–2% isoflurane in oxygen and MRI was performed with a 7.0T 16 cm bore Bruker Biospect MRI system equipped with a quadrature 40-mm coil and a 90-mm gradient coil insert (maximum intensity 360 G/cm) (Bruker Medical GmbH, Ettlingen, Germany). Body temperature and respiratory rate were monitored during the MRI studies using a rectal probe and a gating system for small animals (SA Instruments, Inc., Stony Brook, NY), respectively. T2-weighted spin echo images were obtained with a rapid acquisition with relaxation enhancement (RARE) sequence. Axial and coronal images were obtained for each animal. For axial planes, two set of images were acquired consecutively with and without fat suppression module. For coronal planes, fat images were obtained by applying a frequency selective radiofrequency pulse at a high-field offset of 1000–1100 Hz with respect to the water signal to excite the fat protons only. The acquisition parameters were as follows: repetition time, 3200 ms; echo time 44 ms; number of averages 2; matrix, 256 × 256 within a field of view of 50 × 50 mm; number of slices, 14 for horizontal and 36 for coronal orientations; slice thickness, 1.5 mm, without gap. Image analysis was carried out using NIH ImageJ software (RRID: SCR_003070). For each animal, the total fat volume was calculated and converted to grams by assuming a density of adipose tissue of 0.9 g/mL[103]. Fat mass was expressed as a percentage relative to the total weight of the animal.

In vivo proton magnetic resonance spectroscopy. Non-localized ^{1}H-MRS was performed using a single pulse sequence without water suppression and with a repetition time of 2 s (128 averages). Spectroscopic data were acquired using 2018 points and 7.5 KHz spectral width. The intensities of the water and fat signals were calculated using Mnova software (Mestrelab Research, Santiago de Compostela, Spain) and a relative concentration of fat/water was measured in every case.

Muscle volume. We performed MRI as described[104] using the equipment described above. T2-weighted spin echo images were acquired with a rapid acquisition with relaxation enhancement sequence in axial and coronal orientations with the following parameters: TR=3000 ms, TE=11.57 ms, RARE factor=8, Av=12, FOV=2.5 cm, acquisition matrix=256×256 corresponding to an in-plane resolution of 97×97 μm^2, slice thickness=1 mm without gap between slices. Hind limb images were analyzed with ImageJ software on 5 consecutive slices without gaps, and values from both limbs were obtained and added to generate a single value for each mouse. For axial planes, the first slice was located in the dorsal direction following the one showing the entire length of the tibia. For coronal planes, the stack started at the third slice distal to the tibial plateau. In each slice, regions of interest (ROIs) were manually traced in each projection, and areas of hyper- or hypointense signal corresponding to fat or bone, respectively, were excluded.

Glucose and insulin tolerance tests

Mice were subjected to a glucose-tolerance test after a 6-h fast, receiving an intraperitoneal load of glucose solution (2 g/kg). Glucose levels were determined from blood samples taken from the tail vein at 0, 15, 30, 60, and 120 min using a handheld glucometer (Accu-Chek glucose reader; Roche, Mannheim, Germany). For intraperitoneal insulin-tolerance testing, mice were fasted for 3 h and injected with insulin (0.75 U/kg). Glucose was measured as described above.

Effect of oral succinate on circulating leptin

Ad-*Sucnr1* KO and *Sucnr1*$^{fl/fl}$ mice were fasted overnight before oral administration of 500 mg/kg of disodium succinate (Sigma-Aldrich). Blood samples were collected from the tail after 0, 2, 4, and 6 h post-gavage, and plasma was obtained for leptin determination.

***In vivo* lipolysis inhibition**

Mice fed NCD (8-week-old) or HFD (14-week-old, 8 weeks on HFD-feeding) were treated with 200 μmol/kg of ATGLi (Cayman Chemical, Ann Arbor, MI) or corn oil as vehicle (Sigma-Aldrich) by oral gavage once daily for two weeks. Body weight and food intake were monitored daily. At the end of the study, animals were fasted overnight, killed by cervical dislocation, and tissues were collected.

Chronic leptin treatment

Ad-*Sucnr1* KO mice (8-week-old) fed NCD were intraperitoneally injected with 0.5 mg/kg leptin (Sigma-Aldrich) or PBS (as vehicle) twice daily (8:00 am and 7:00 pm) for 4 weeks. Body weight and food intake were monitored daily before leptin injection. Control mice were pair-fed to leptin-treated mice. At the end of the study, animals were fasted overnight, killed by cervical dislocation, and tissues were collected.

Feeding studies and leptin sensitivity tests

To study the gene expression in the transition from fasted to fed state, mice were fasted for 24 h, then one-half of the mice were sacrificed and the other one-half were refed for 12 h before sacrifice. For western-blot studies, mice were singly housed and acclimatized for 3 days prior to the study. Mice were fasted for 24 h, then one-half of the mice were sacrificed and the other one-half were refed for 20 minutes. For leptin sensitivity tests, mice were acclimatized by subjecting them to handling and sham injections. Mice were fasted overnight and intraperitoneally injected with 3 μg/g of mouse leptin (R&D Systems, Minneapolis, MN) or PBS. After 1 h, mice were sacrificed. In all cases, the hypothalamus was collected and immediately frozen. Alternatively, leptin sensitivity on body weight and food intake was analyzed in Ad-*Sucnr1* KO and *Sucnr1*$^{fl/fl}$

mice intraperitoneally injected with 0.5 mg/kg leptin or PBS (as vehicle) twice daily (8:00 am and 7:00 pm) for 4 days, and body weight and food intake were monitored daily before leptin injection.

Microcomputed tomography

Tibias from 22-week-old NCD-fed mice, and from mice fed HFD for 13 weeks (21-weeks old) were dissected, cleaned of soft tissue, and fixed in 4% paraformaldehyde (PFA; Sigma-Aldrich) for 24 h at 4°C. Samples were placed in PBS for 24 h at 4ºC and subsequently placed in 20% sodium azide (Thermo Scientific, Rockford, IL) diluted in PBS at 4ºC until analysis. High-resolution images from the tibia were acquired using a computerized microtomography imaging system (SkyScan 1272, Bruker microCT, Kontich, Belgium) in accordance with recommendations from the American Society of Bone and Mineral Research. Samples were scanned in air at 70 kV and a power of 10 W (143 μA) with an exposure time of 2700 ms, using a 1-mm aluminum filter and an isotropic voxel size of 11 μm. Two-dimensional images were obtained every 1º of a 180º rotation and were subsequently reconstructed using NRecon reconstruction software and analyzed with a CT-Analyzer (SkyScan). For trabecular measurements manual ROIs were selected, starting 0.6 mm from the growth plate of the tibiae and extending to the diaphysis for 2 mm. For cortical parameters analysis, a 3-mm section starting from the bifurcation of the fibula was selected. A Gaussian noise filter was applied for reconstruction and a global binary threshold was manually established at 15 for trabecular analysis and at 50 for cortical analysis.

***Ex vivo* lipolysis determination**

Mouse eWAT tissues (0.8 g) were cultured in 24-well plates with KRBH buffer supplemented with 0.1% free-fatty acid-BSA. Lipolysis was induced with 1 μM isoproterenol (Sigma-Aldrich) and explants were also treated with 100 μM *c*ESA for 3 h. Lipolysis was determined by measuring glycerol released in the culture medium (Free Glycerol Reagent, Sigma-Aldrich).

Brown adipocyte differentiation of mASCs

Mouse ASCs were cultured in 6-well plates with a brown adipocyte induction medium containing DMEM/F12 supplemented with 10% FBS, 15 mM HEPES, 1 nM insulin, 100 μM IBMX, 1 μM dexamethasone, and 3 μM rosiglitazone. After 4 days, the medium was replaced with the absence of insulin until day 10 of differentiation. To evaluate lipids, cells were fixed with 4% PFA for 15 min, washed with distilled water, and stained for 45 min with Oil Red O (Sigma-Aldrich). Lipid vesicles were photographed using a light microscope equipped with a Zeiss AxioCam MRM (Zeiss, Germany) and ZEN Digital Imaging for Light Microscopy v3.1 software (blue edition;

RRID: SCR_013672; Zeiss). The stain was eluted using isopropanol for 5 min and the optical density was read at 540 nm.

Osteoblast differentiation of BM-MSCs

BM-MSCs were cultured in 12-well plates with DMEM-High Glucose containing 10 mM β-glycerol phosphate, 100 mM dexamethasone, and 0.5 mM L-ascorbic acid (all from Sigma-Aldrich) for 2 weeks. Differentiated BM-MSCs were fixed in 4% PFA and washed in distilled water. The cells were incubated with 1% Alizarin red S staining solution (pH 4.1; Sigma-Aldrich) at room temperature for 45 min. Excess staining was washed in distilled water and mineralization alterations were photographed using a light microscope equipped with a Zeiss AxioCam MRM and ZEN Digital Imaging for Light Microscopy v3.1 software (blue edition). The stain was eluted with 10% hexadecylpyridinium chloride (Sigma-Aldrich) and the optical density was read at 540 nm.

Cell fractionation assay

3T3-L1 differentiated adipocytes were lysed in homogenization buffer (20 mM Tris-HCl, 2 mM EDTA, 2 mM EGTA, 1 mM phenylmethylsulfonyl fluoride (PMSF), 10 mM 2-mercaptoethanol, 10 µg/L aprotinin, and 10 µg/mL leupeptin) followed by mechanical disruption using a Dounce homogenizer. Total lysates were centrifuged at 1300 rpm for 10 min after which the pellets containing nuclei were collected.

Biochemical parameters

Plasma triglycerides and non-esterified fatty acids were determined enzymatically using commercial kits adapted to a COBAS 6000 autoanalyzer (Roche Diagnostics, Rotkreuz, Switzerland). Leptin levels were determined from plasma or cell conditioned medium using the Leptin Quantikine ELISA (mouse or human) (R&D Systems, Minneapolis, MN). For succinate determination, human plasma samples were filtered (10-kDa) and succinate levels were measured using the fluorometric Succinate Assay Kit (Sigma Aldrich), following the manufacturer's instructions[10]. Tissular succinate accumulation was determined in 20 mg of eWAT, using the Succinate Colorimetric Assay Kit (Sigma-Aldrich), following the manufacturer's instructions.

Gene-expression analysis

Total RNA was extracted from tissues or cells using TRIzol Reagent (Invitrogen, Carlsbad, CA). cDNA was generated using the High-capacity cDNA Reverse Transcription kit (Applied Biosystems, Carlsbad, CA), and was subjected to quantitative real-time PCR amplification on a 7900HT Fast Real-Time PCR System using the TaqMan Gene Expression Assay (Applied Biosystems; Table S6). *B2m* and *RNA18S5* were used as housekeeping genes for mice and human

samples, respectively. Relative expression was calculated using the comparative Ct method ($2^{-\Delta\Delta Ct}$).

Transcriptome analysis by RNA sequencing

RNA sequencing was performed on vWAT from 5 *Sucnr1*$^{fl/fl}$ mice and 5 Ad-*Sucnr1* KO mice. RNA was extracted using TRIzol reagent and further purified/DNase treated with the RNeasy Mini Kit (Qiagen, Hilden, Germany). Samples were sequenced at Centro Nacional de Análisis Genómico (CNAG-CRG, Barcelona, Spain). Libraries were prepared using the TruSeq Stranded Total RNA Library Prep kit (Human/Mouse/Rat 96 samples, Illumina, San Diego, CA) according to the manufacturer's protocol, to convert total RNA into a library of template molecules of known strand origin and suitable for subsequent cluster generation and DNA sequencing. Briefly, 300 ng of total RNA were used to remove ribosomal RNA (rRNA) using biotinylated, target-specific oligos combined with Ribo-Zero rRNA removal beads. An extra step using Sera-Mag beads (GE Healthcare/Thermo, Chicago, IL) was added to Illumina protocol to improve rRNA depletion. After the rRNA is depleted, the remaining RNA is purified with RNAClean XP beads (Beckman Coulter, Brea, CA). Following purification, the RNA is fragmented into small pieces using divalent cations under elevated temperature, and primed with random hexamers for cDNA synthesis. Then, the cleaved RNA fragments were copied into first strand cDNA using reverse transcriptase (SuperScript II, Invitrogen, Carlsbad, CA) and random primers. After that, second strand cDNA was synthesized, removing the RNA template and synthesizing a replacement strand, incorporating dUTP in place of dTTP to generate dscDNA using DNA Polymerase I and RNase H. These cDNA fragments then had the addition of a single 'A' base to the 3'ends of the blunt fragments to prevent them from ligating to one another during the adapter ligation. A corresponding single T nucleotide on the 3' end of the adapter provides a complementary overhang for ligating the adapter to the fragments ensuring a low rate of chimera (concatenated template) formation. Subsequent ligation of the multiple indexing adapter to the ends of the dscDNA was performed after A-tailing. Finally, PCR selectively enriched those DNA fragments that had adapter molecules on both ends and amplified the amount of DNA in the library. The PCR was performed with a PCR Primer Cocktail that anneals to the ends of the adapters. Final libraries were analyzed using Bioanalyzer DNA 1000 or Fragment Analyzer Standard Sensitivity (Agilent, Santa Clara, CA) to estimate the quantity and validate the size distribution, and were then quantified by qPCR using the KAPA Library Quantification Kit KK4835 (Roche, Basel, Switzerland) prior to sequencing. Libraries were sequenced 1 x 51+8+8 bp to at least 60 million reads per sample on the Illumina NextSeq2000 platform.

Read files for each sample were subsequently downloaded and collated into a single FASTQ file. FastQC (version 0.11.9; RRID: SCR_014583; BaseSpace Labs, Illumina) was used to evaluate

the quality of raw read data and identify problematic features (inappropriate GC content, over-represented sequences, and/or low-quality scores). Reads were mapped against *Mus musculus* reference genome (GRCm38.p6) using STAR software (v2.5.2; RRID: SCR_004463)[105], and were assigned to genes using feature Counts from the Bioconductor package Rsubread (v2.8.2; RRID: SCR_016945)[106]. All RNA sequencing data have been uploaded to Gene Expression Omnibus (GEO) with the accession number GSE200749.

Western blotting

Cells and tissues were lysed and homogenized in M-PER buffer (Thermo Scientific) containing Halt Protease and Phosphatase Inhibitor Cocktails (Thermo Scientific). Protein concentration was determined with the BCA Protein Assay Kit (Thermo Scientific). Equal amounts of total protein were separated in SDS-polyacrylamide gel electrophoresis, transferred to Immobilon-P PDVF membranes (Merck Millipore, Burlington, MA) and blocked. Immunoblot analysis was performed with polyclonal antibodies against phospho(p)-AKT (Ser473) (RRID: AB_331168), p-AKT (Thr308) (RRID: AB_329828), p-C/EBPα (Ser21) (RRID: AB_2077882), p-GSK3α/β (Ser21/9) (RRID: AB_329830), p-p44/42 MAPK (Erk1/2) (Thr202/Tyr204) (RRID: AB_331646), and p-SAPK/JNK (Thr183/Tyr185) (RRID: AB_331659), p-BMAL1 (Ser42) (RRID: AB_2798348), and BMAL (RRID: AB_10675117); or with monoclonal antibodies against p-AMPKα (Thr172) (RRID: AB_331250), p-IGF-I Receptor β (Tyr1135/1136)/Insulin Receptor β (Tyr1150/1151) (19H7) (RRID: AB_331253), p-p38 MAPK (Thr180/Tyr182) (RRID: AB_2139682), and p-STAT3 (Tyr705) (RRID: AB_2491009). All antibodies were from Cell Signaling Technology (Danvers, MA) except for a monoclonal antibody against β-ACTIN (Sigma-Aldrich; RRID: AB_476692) and a polyclonal anti-LAMIN A/C (Santa Cruz Biotechnology, Dallas, TX; RRID: AB_648152), which were used as loading controls, and the anti-BMAL1 antibody (Abcam, Cambridge, UK). Membranes were incubated with the respective anti-HRP secondary antibodies and visualized with the Immobilon ECL Ultra Western HRP Substrate (Merck Millipore). Band intensity was captured using the iBright CL1000 Imaging System equipped with iBright Analysis Software (RRID: SCR_017632; Invitrogen, Waltham, MA).

Histology

Blocks of paraffin-embedded tissues from mice were sectioned at 5-µm, deparaffinized, rehydrated, and stained with Harris hematoxylin (StatLab Medical Products, McKinney, TX) and eosin (Sigma-Aldrich). For UCP1 immunohistochemistry, tissue sections were heated for 10 min in 10 mM Tris, 1 mM EDTA, and 0.05% Tween-20 (Sigma-Aldrich), and then blocked for 30 min with a solution of 1% H_2O_2 (Sigma-Aldrich). To block non-specific binding, sections were

incubated with 0.2% gelatin (Sigma-Aldrich), 2% BSA, and 2% FBS in PBS for 30 min at room temperature. Incubation with the primary antibody (1:500 UCP1, polyclonal; Abcam; RRID: AB_2241462) was performed overnight, followed by incubation with a secondary anti-rabbit antibody (1:250, Amersham ECL, GE Healthcare) for 1 h, and with Vectastain ABC (Vector Laboratories, Burlingame, CA) for 1 h (all incubations were performed in a humid chamber at room temperature). Finally, the slides were stained with the DAB peroxidase substrate kit (Vector Laboratories) for 4 min and counterstained with Mayer's hematoxylin solution (Sigma-Aldrich) for 1.5 min. Images were viewed using a Leica DM4 B microscope (Wetzlar, Germany) and image acquisition was performed using Leica microsystems imaging software. Adipocyte size analysis was performed using the Adiposoft plug-in of ImageJ.

For bone histological preparations, samples were fixed in 4% PFA for 24 h at 4ºC, decalcified in 14% EDTA (pH 7.4) for 6 weeks, and embedded in paraffin. Samples were cut into 5-µm sections and stained with H&E for osteocyte and osteoblast quantification, or with tartrate-resistant acid phosphatase (TRAP) for osteoclasts. For TRAP staining, deparaffinized and rehydrated slides were incubated with naphthol AS-BI phosphate (Sigma-Aldrich) for 1 h at 37°C and osteoclasts were developed with pararosaniline hydrochloride (Sigma-Aldrich) for 3 min. The rest of the tissue was counterstained with 0.02% fast green solution (Sigma-Aldrich) for 45 seconds. Cells were quantified from images captured using Nikon Eclipse E800 Micorscope (RRID: SCR_020326; Nikon, Tokyo, Japan).

Luciferase reporter assay

To analyze BMAL1 promoter activity, 10 ng of pBMAL-LUC (kindly provided by S. Yamazaki, UT Southwestern Medical Center; and K. Eckel-Mahan, University of Texas)[107] and pCMV6-human SUCNR1 (GFP-tagged; Origene, Rockville, MD) were co-transfected into $10^5/cm^2$ HEK293 cells using 0.15 µL of Lipofectamine 3000, according to the manufacturer's protocol. Twenty-four hours post-transfection, cells were treated with SR1078 (Calbiochem)–a selective agonist of retinoic acid receptor-related orphan receptor α/γ (RORα/RORγ)–which is a BMAL1 activator. Forty-three hours post-transfection, cells were deprived of serum for 2 h with FBS-free medium containing 0.2% BSA, and treated with 100 µM *c*ESA. Luminescence was measured 48 h post-transfection using the Nano-Glo® Dual-Luciferase® Reporter Assay System (Promega, Madison, WI), according to the manufacturer's manual.

The pGL3-Basic plasmid (promoter-less; Promega) was used in each experiment to determine the basal levels of luciferase expression (designated as Luc). Cells were also co-transfected with pNL1.1.PGK[Nluc/PGK] vector (Promega) and NanoLuc® Luciferase measurements were used to normalize experiments for transfection efficiency. Each construct was tested in three

independent transfection experiments. Luminescence was read with the Varioscan Lux plate reader (Thermo Scientific), in a white 96-well plate.

QUANTIFICATION AND STATISTICAL ANALYSIS

Shapiro-Wilk normality tests were performed to assess Gaussian distribution. When data followed Gaussian distribution, the unpaired two-tailed t-test was used to compare differences between two groups, whereas a one-way ANOVA with Dunnet's post-test was used to compare groups to a control group. For data that did not follow Gaussian distribution, the non-parametric Mann-Whitney two-tailed test was used to compare the differences between two groups, whereas the Kruskal-Wallis test followed by Dunn's multiple comparisons test was used to compare groups to a control group. Two-way ANOVA was performed in time-course analyses of body weight, GTT and ITT. GraphPad Prism 8 software for Windows (RRID: SCR_002798; San Diego, CA) was used to perform all statistical analyses. A $p<0.05$ was considered statistically significant. In box-and-whiskers plots, the center line depicts the median, box limits represent upper and lower quartiles, and whiskers show the min to max range. In time-course graphs, data are presented as mean±SEM. In violin plots, lines represent median and quartiles.

For mass-dependent measurements such as energy expenditure and food intake, a Generalized Linear Model (GLM) was performed to test for a significant interaction between genotype and body weight as per recommendations by Mina and colleagues[108], using R software v4.2.0[109] (RRID: SCR_001905). If no statistically significant interaction effect was observed, we then performed an ANCOVA without interaction and with body weight as the covariate. In the special case of a significant genotype effect but no significant body weight effect, the model was simplified to one-way ANOVA. Indirect calorimetry measurements not associated with mass, such as RER, were analyzed by one-way ANOVA. For time-course statistical analysis, measurements were averaged per animal on the second day, allowing for one day of acclimatization. Regression-based plots was performed using ggplot2 R package v3.3.6[110] (RRID: SCR_014601) and ggpubr R package v0.4.0 (RRID: SCR_021139).

For clinical data, associations between quantitative variables were evaluated using the Spearman correlation, and multiple linear regression analyses were employed (stepwise forward selection procedures) to determine which variables were independent factors. All variables associated in the univariate analysis with leptin gene expression were included in their respective models. Regression analyses were performed using IBM SPSS Statistics (v27.0; RRID: SCR_002865; Armonk, NY).

RNA sequencing analysis and data visualization were performed using R software v4.1.2[109]. Principal component analysis was conducted using the limma package (v3.50.1; RRID: SCR_010943)[111] to investigate technical batch noise. No sample was excluded from analysis. Normalization and differential expression analysis were performed using the R/Bioconductor package DESeq2 (v1.34.0; RRID: SCR_015687)[112] and *p*-values were adjusted for multiple comparisons using the Benjamini-Hochberg procedure (fold change>1.25, adjusted $p<0.05$). Pathway enrichment analysis was performed with rotation gene set tests/Gene Set Analysis (ROAST-GSA, version 1.03.2), a hybrid of methods that combines the statistical inference based on limma and rotations from ROAST[113] and the re-standardized MaxMean statistic from GSA[114]. The Bioconductor R package org.Hs.eg.db (RRID:SCR_006442) was used to annotate genes according to Kyoto Encyclopedia of Genes and Genomes (KEGG) pathways[115]. *P*-values were adjusted for multiple comparisons using the Benjamini-Hochberg procedure and enriched pathways were considered significantly different if the adjusted *p*-value <0.25.

REFERENCES

1. Fernández-Veledo, S., Ceperuelo-Mallafré, V., and Vendrell, J. (2021). Rethinking succinate: an unexpected hormone-like metabolite in energy homeostasis. Trends Endocrinol. Metab. TEM *32*, 680–692. 10.1016/j.tem.2021.06.003.

2. Tretter, L., Patocs, A., and Chinopoulos, C. (2016). Succinate, an intermediate in metabolism, signal transduction, ROS, hypoxia, and tumorigenesis. Biochim. Biophys. Acta *1857*, 1086–1101. 10.1016/j.bbabio.2016.03.012.

3. McCreath, K.J., Espada, S., Gálvez, B.G., Benito, M., de Molina, A., Sepúlveda, P., and Cervera, A.M. (2015). Targeted disruption of the SUCNR1 metabolic receptor leads to dichotomous effects on obesity. Diabetes *64*, 1154–1167. 10.2337/db14-0346.

4. Regard, J.B., Sato, I.T., and Coughlin, S.R. (2008). Anatomical profiling of G protein-coupled receptor expression. Cell *135*, 561–571. 10.1016/j.cell.2008.08.040.

5. Rubic, T., Lametschwandtner, G., Jost, S., Hinteregger, S., Kund, J., Carballido-Perrig, N., Schwärzler, C., Junt, T., Voshol, H., Meingassner, J.G., et al. (2008). Triggering the succinate receptor GPR91 on dendritic cells enhances immunity. Nat. Immunol. *9*, 1261–1269. 10.1038/ni.1657.

6. Lei, W., Ren, W., Ohmoto, M., Urban, J.F., Matsumoto, I., Margolskee, R.F., and Jiang, P. (2018). Activation of intestinal tuft cell-expressed Sucnr1 triggers type 2 immunity in the mouse small intestine. Proc. Natl. Acad. Sci. U. S. A. *115*, 5552–5557. 10.1073/pnas.1720758115.

7. Littlewood-Evans, A., Sarret, S., Apfel, V., Loesle, P., Dawson, J., Zhang, J., Muller, A., Tigani, B., Kneuer, R., Patel, S., et al. (2016). GPR91 senses extracellular succinate released from inflammatory macrophages and exacerbates rheumatoid arthritis. J. Exp. Med. *213*, 1655–1662. 10.1084/jem.20160061.

8. Peruzzotti-Jametti, L., Bernstock, J.D., Vicario, N., Costa, A.S.H., Kwok, C.K., Leonardi, T., Booty, L.M., Bicci, I., Balzarotti, B., Volpe, G., et al. (2018). Macrophage-Derived Extracellular Succinate Licenses Neural Stem Cells to Suppress Chronic Neuroinflammation. Cell Stem Cell *22*, 355-368.e13. 10.1016/j.stem.2018.01.020.

9. Sadagopan, N., Li, W., Roberds, S.L., Major, T., Preston, G.M., Yu, Y., and Tones, M.A. (2007). Circulating succinate is elevated in rodent models of hypertension and metabolic disease. Am. J. Hypertens. *20*, 1209–1215. 10.1016/j.amjhyper.2007.05.010.

10. Serena, C., Ceperuelo-Mallafré, V., Keiran, N., Queipo-Ortuño, M.I., Bernal, R., Gomez-Huelgas, R., Urpi-Sarda, M., Sabater, M., Pérez-Brocal, V., Andrés-Lacueva, C., et al. (2018). Elevated circulating levels of succinate in human obesity are linked to specific gut microbiota. ISME J. *12*, 1642–1657. 10.1038/s41396-018-0068-2.

11. Macias-Ceja, D.C., Ortiz-Masiá, D., Salvador, P., Gisbert-Ferrándiz, L., Hernández, C., Hausmann, M., Rogler, G., Esplugues, J.V., Hinojosa, J., Alós, R., et al. (2019). Succinate receptor mediates intestinal inflammation and fibrosis. Mucosal Immunol. *12*, 178–187. 10.1038/s41385-018-0087-3.

12. Osuna-Prieto, F.J., Martinez-Tellez, B., Ortiz-Alvarez, L., Di, X., Jurado-Fasoli, L., Xu, H., Ceperuelo-Mallafré, V., Núñez-Roa, C., Kohler, I., Segura-Carretero, A., et al. (2021). Elevated plasma succinate levels are linked to higher cardiovascular disease risk factors in young adults. Cardiovasc. Diabetol. *20*, 151. 10.1186/s12933-021-01333-3.

13. Reddy, A., Bozi, L.H.M., Yaghi, O.K., Mills, E.L., Xiao, H., Nicholson, H.E., Paschini, M., Paulo, J.A., Garrity, R., Laznik-Bogoslavski, D., et al. (2020). pH-Gated Succinate Secretion Regulates Muscle Remodeling in Response to Exercise. Cell *183*, 62-75.e17. 10.1016/j.cell.2020.08.039.

14. Mills, E.L., Pierce, K.A., Jedrychowski, M.P., Garrity, R., Winther, S., Vidoni, S., Yoneshiro, T., Spinelli, J.B., Lu, G.Z., Kazak, L., et al. (2018). Accumulation of succinate controls activation of adipose tissue thermogenesis. Nature *560*, 102–106. 10.1038/s41586-018-0353-2.

15. Astiarraga, B., Martínez, L., Ceperuelo-Mallafré, V., Llauradó, G., Terrón-Puig, M., Rodríguez, M.M., Casajoana, A., Pellitero, S., Megía, A., Vilarrasa, N., et al. (2020). Impaired Succinate Response to a Mixed Meal in Obesity and Type 2 Diabetes Is Normalized After Metabolic Surgery. Diabetes Care *43*, 2581–2587. 10.2337/dc20-0460.

16. Harvey, I., Boudreau, A., and Stephens, J.M. (2020). Adipose tissue in health and disease. Open Biol. *10*, 200291. 10.1098/rsob.200291.

17. Friedman, J.M. (2019). Leptin and the endocrine control of energy balance. Nat. Metab. *1*, 754–764. 10.1038/s42255-019-0095-y.

18. Picó, C., Palou, M., Pomar, C.A., Rodríguez, A.M., and Palou, A. (2021). Leptin as a key regulator of the adipose organ. Rev. Endocr. Metab. Disord.

19. Levine, J.A., Eberhardt, N.L., and Jensen, M.D. (1999). Leptin responses to overfeeding: relationship with body fat and nonexercise activity thermogenesis. J. Clin. Endocrinol. Metab. *84*, 2751–2754. 10.1210/jcem.84.8.5910.

20. Jensen, M.D., Hensrud, D., O'Brien, P.C., and Nielsen, S. (1999). Collection and interpretation of plasma leptin concentration data in humans. Obes. Res. *7*, 241–245. 10.1002/j.1550-8528.1999.tb00402.x.

21. Elimam, A., and Marcus, C. (2002). Meal timing, fasting and glucocorticoids interplay in serum leptin concentrations and diurnal profile. Eur. J. Endocrinol. *147*, 181–188. 10.1530/eje.0.1470181.

22. Schneeberger, M., Gomis, R., and Claret, M. (2014). Hypothalamic and brainstem neuronal circuits controlling homeostatic energy balance. J. Endocrinol. *220*, T25-46. 10.1530/JOE-13-0398.

23. Genchi, V.A., D'Oria, R., Palma, G., Caccioppoli, C., Cignarelli, A., Natalicchio, A., Laviola, L., Giorgino, F., and Perrini, S. (2021). Impaired Leptin Signalling in Obesity: Is Leptin a New Thermolipokine? Int. J. Mol. Sci. *22*, 6445. 10.3390/ijms22126445.

24. Obradovic, M., Sudar-Milovanovic, E., Soskic, S., Essack, M., Arya, S., Stewart, A.J., Gojobori, T., and Isenovic, E.R. (2021). Leptin and Obesity: Role and Clinical Implication. Front. Endocrinol. *12*, 585887. 10.3389/fendo.2021.585887.

25. Zeigerer, A., Rodeheffer, M.S., McGraw, T.E., and Friedman, J.M. (2008). Insulin regulates leptin secretion from 3T3-L1 adipocytes by a PI 3 kinase independent mechanism. Exp. Cell Res. *314*, 2249–2256. 10.1016/j.yexcr.2008.04.003.

26. Lee, K.N., Jeong, I.C., Lee, S.J., Oh, S.H., and Cho, M.Y. (2001). Regulation of leptin gene expression by insulin and growth hormone in mouse adipocytes. Exp. Mol. Med. *33*, 234–239. 10.1038/emm.2001.38.

27. Lee, M.-J., Wang, Y., Ricci, M.R., Sullivan, S., Russell, C.D., and Fried, S.K. (2007). Acute and chronic regulation of leptin synthesis, storage, and secretion by insulin and dexamethasone in human adipose tissue. Am. J. Physiol. Endocrinol. Metab. *292*, E858-864. 10.1152/ajpendo.00439.2006.

28. Jahng, J.W., Kim, N.Y., Ryu, V., Yoo, S.B., Kim, B.-T., Kang, D.-W., and Lee, J.-H. (2008). Dexamethasone reduces food intake, weight gain and the hypothalamic 5-HT

concentration and increases plasma leptin in rats. Eur. J. Pharmacol. *581*, 64–70. 10.1016/j.ejphar.2007.11.029.

29. Keller, P., Keller, C., Steensberg, A., Robinson, L.E., and Pedersen, B.K. (2005). Leptin gene expression and systemic levels in healthy men: effect of exercise, carbohydrate, interleukin-6, and epinephrine. J. Appl. Physiol. Bethesda Md 1985 *98*, 1805–1812. 10.1152/japplphysiol.00592.2004.

30. Carulli, L., Ferrari, S., Bertolini, M., Tagliafico, E., and Del Rio, G. (1999). Regulation of ob gene expression: evidence for epinephrine-induced suppression in human obesity. J. Clin. Endocrinol. Metab. *84*, 3309–3312. 10.1210/jcem.84.9.6007.

31. An, Y.A., Chen, S., Deng, Y., Wang, Z.V., Funcke, J.-B., Shah, M., Shan, B., Gordillo, R., Yoshino, J., Klein, S., et al. (2021). The mitochondrial dicarboxylate carrier prevents hepatic lipotoxicity by inhibiting white adipocyte lipolysis. J. Hepatol. *75*, 387–399. 10.1016/j.jhep.2021.03.006.

32. Gilissen, J., Jouret, F., Pirotte, B., and Hanson, J. (2016). Insight into SUCNR1 (GPR91) structure and function. Pharmacol. Ther. *159*, 56–65. 10.1016/j.pharmthera.2016.01.008.

33. van Diepen, J.A., Robben, J.H., Hooiveld, G.J., Carmone, C., Alsady, M., Boutens, L., Bekkenkamp-Grovenstein, M., Hijmans, A., Engelke, U.F.H., Wevers, R.A., et al. (2017). SUCNR1-mediated chemotaxis of macrophages aggravates obesity-induced inflammation and diabetes. Diabetologia *60*, 1304–1313. 10.1007/s00125-017-4261-z.

34. Keiran, N., Ceperuelo-Mallafré, V., Calvo, E., Hernández-Alvarez, M.I., Ejarque, M., Núñez-Roa, C., Horrillo, D., Maymó-Masip, E., Rodríguez, M.M., Fradera, R., et al. (2019). SUCNR1 controls an anti-inflammatory program in macrophages to regulate the metabolic response to obesity. Nat. Immunol. *20*, 581–592. 10.1038/s41590-019-0372-7.

35. Parajuli, N., Takahara, S., Matsumura, N., Kim, T.T., Ferdaoussi, M., Migglautsch, A.K., Zechner, R., Breinbauer, R., Kershaw, E.E., and Dyck, J.R.B. (2018). Atglistatin ameliorates functional decline in heart failure via adipocyte-specific inhibition of adipose triglyceride lipase. Am. J. Physiol. Heart Circ. Physiol. *315*, H879–H884. 10.1152/ajpheart.00308.2018.

36. Monfort-Ferré, D., Caro, A., Menacho, M., Martí, M., Espina, B., Boronat-Toscano, A., Nuñez-Roa, C., Seco, J., Bautista, M., Espín, E., et al. (2022). The Gut Microbiota Metabolite Succinate Promotes Adipose Tissue Browning in Crohn's Disease. J. Crohns Colitis *16*, 1571–1583. 10.1093/ecco-jcc/jjac069.

37. Mazess, R.B., Peppler, W.W., and Gibbons, M. (1984). Total body composition by dual-photon (153Gd) absorptiometry. Am. J. Clin. Nutr. *40*, 834–839. 10.1093/ajcn/40.4.834.

38. Chen, Q., Shou, P., Zheng, C., Jiang, M., Cao, G., Yang, Q., Cao, J., Xie, N., Velletri, T., Zhang, X., et al. (2016). Fate decision of mesenchymal stem cells: adipocytes or osteoblasts? Cell Death Differ. *23*, 1128–1139. 10.1038/cdd.2015.168.

39. Skowronski, A.A., Shaulson, E.D., Leibel, R.L., and LeDuc, C.A. (2022). The postnatal leptin surge in mice is variable in both time and intensity and reflects nutritional status. Int. J. Obes. *46*, 39–49. 10.1038/s41366-021-00957-5.

40. Ruvolo, P.P., Qiu, Y., Coombes, K.R., Zhang, N., Neeley, E.S., Ruvolo, V.R., Hail, N., Borthakur, G., Konopleva, M., Andreeff, M., et al. (2015). Phosphorylation of GSK3α/β correlates with activation of AKT and is prognostic for poor overall survival in acute myeloid leukemia patients. BBA Clin. *4*, 59–68. 10.1016/j.bbacli.2015.07.001.

41. Steinberg, G.R., and Carling, D. (2019). AMP-activated protein kinase: the current landscape for drug development. Nat. Rev. Drug Discov. *18*, 527–551. 10.1038/s41573-019-0019-2.

42. Hwang, C.S., Mandrup, S., MacDougald, O.A., Geiman, D.E., and Lane, M.D. (1996). Transcriptional activation of the mouse obese (ob) gene by CCAAT/enhancer binding protein alpha. Proc. Natl. Acad. Sci. U. S. A. *93*, 873–877. 10.1073/pnas.93.2.873.

43. Miller, S.G., De Vos, P., Guerre-Millo, M., Wong, K., Hermann, T., Staels, B., Briggs, M.R., and Auwerx, J. (1996). The adipocyte specific transcription factor C/EBPalpha modulates human ob gene expression. Proc. Natl. Acad. Sci. U. S. A. *93*, 5507–5511. 10.1073/pnas.93.11.5507.

44. Kettner, N.M., Mayo, S.A., Hua, J., Lee, C., Moore, D.D., and Fu, L. (2015). Circadian Dysfunction Induces Leptin Resistance in Mice. Cell Metab. *22*, 448–459. 10.1016/j.cmet.2015.06.005.

45. Otway, D.T., Frost, G., and Johnston, J.D. (2009). Circadian rhythmicity in murine pre-adipocyte and adipocyte cells. Chronobiol. Int. *26*, 1340–1354. 10.3109/07420520903412368.

46. Shea, S.A., Hilton, M.F., Orlova, C., Ayers, R.T., and Mantzoros, C.S. (2005). Independent circadian and sleep/wake regulation of adipokines and glucose in humans. J. Clin. Endocrinol. Metab. *90*, 2537–2544. 10.1210/jc.2004-2232.

47. Lipton, J.O., Yuan, E.D., Boyle, L.M., Ebrahimi-Fakhari, D., Kwiatkowski, E., Nathan, A., Güttler, T., Davis, F., Asara, J.M., and Sahin, M. (2015). The Circadian Protein BMAL1 Regulates Translation in Response to S6K1-Mediated Phosphorylation. Cell *161*, 1138–1151. 10.1016/j.cell.2015.04.002.

48. Knight, Z.A., Hannan, K.S., Greenberg, M.L., and Friedman, J.M. (2010). Hyperleptinemia is required for the development of leptin resistance. PloS One *5*, e11376. 10.1371/journal.pone.0011376.

49. Longo, K.A., Charoenthongtrakul, S., Giuliana, D.J., Govek, E.K., McDonagh, T., Qi, Y., DiStefano, P.S., and Geddes, B.J. (2008). Improved insulin sensitivity and metabolic flexibility in ghrelin receptor knockout mice. Regul. Pept. *150*, 55–61. 10.1016/j.regpep.2008.03.011.

50. Gilbertson, N.M., Eichner, N.Z.M., Francois, M., Gaitán, J.M., Heiston, E.M., Weltman, A., and Malin, S.K. (2018). Glucose Tolerance is Linked to Postprandial Fuel Use Independent of Exercise Dose. Med. Sci. Sports Exerc. *50*, 2058–2066. 10.1249/MSS.0000000000001667.

51. Ahmed, K., Tunaru, S., Tang, C., Müller, M., Gille, A., Sassmann, A., Hanson, J., and Offermanns, S. (2010). An autocrine lactate loop mediates insulin-dependent inhibition of lipolysis through GPR81. Cell Metab. *11*, 311–319. 10.1016/j.cmet.2010.02.012.

52. Zhang, G., Li, R., Li, W., Yang, S., Sun, Q., Yin, H., Wang, C., Hou, B., Wang, H., Yu, L., et al. (2021). Toll-like receptor 3 ablation prevented high-fat diet-induced obesity and metabolic disorder. J. Nutr. Biochem. *95*, 108761. 10.1016/j.jnutbio.2021.108761.

53. Tunaru, S., Kero, J., Schaub, A., Wufka, C., Blaukat, A., Pfeffer, K., and Offermanns, S. (2003). PUMA-G and HM74 are receptors for nicotinic acid and mediate its anti-lipolytic effect. Nat. Med. *9*, 352–355. 10.1038/nm824.

54. Bartelt, A., and Heeren, J. (2014). Adipose tissue browning and metabolic health. Nat. Rev. Endocrinol. *10*, 24–36. 10.1038/nrendo.2013.204.

55. Kazak, L., Chouchani, E.T., Lu, G.Z., Jedrychowski, M.P., Bare, C.J., Mina, A.I., Kumari, M., Zhang, S., Vuckovic, I., Laznik-Bogoslavski, D., et al. (2017). Genetic Depletion of Adipocyte Creatine Metabolism Inhibits Diet-Induced Thermogenesis and Drives Obesity. Cell Metab. *26*, 660-671.e3. 10.1016/j.cmet.2017.08.009.

56. Gao, H., Guo, Y., Yan, Q., Yang, W., Li, R., Lin, S., Bai, X., Liu, C., Chen, D., Cao, H., et al. (2019). Lipoatrophy and metabolic disturbance in mice with adipose-specific deletion of kindlin-2. JCI Insight *4*, 128405. 10.1172/jci.insight.128405.

57. Corsa, C.A.S., Walsh, C.M., Bagchi, D.P., Foss Freitas, M.C., Li, Z., Hardij, J., Granger, K., Mori, H., Schill, R.L., Lewis, K.T., et al. (2021). Adipocyte-Specific Deletion of Lamin A/C Largely Models Human Familial Partial Lipodystrophy Type 2. Diabetes *70*, 1970–1984. 10.2337/db20-1001.

58. Urs, S., Venkatesh, D., Tang, Y., Henderson, T., Yang, X., Friesel, R.E., Rosen, C.J., and Liaw, L. (2010). Sprouty1 is a critical regulatory switch of mesenchymal stem cell lineage allocation. FASEB J. Off. Publ. Fed. Am. Soc. Exp. Biol. *24*, 3264–3273. 10.1096/fj.10-155127.

59. Fazeli, P.K., Horowitz, M.C., MacDougald, O.A., Scheller, E.L., Rodeheffer, M.S., Rosen, C.J., and Klibanski, A. (2013). Marrow fat and bone--new perspectives. J. Clin. Endocrinol. Metab. *98*, 935–945. 10.1210/jc.2012-3634.

60. Upadhyay, J., Farr, O.M., and Mantzoros, C.S. (2015). The role of leptin in regulating bone metabolism. Metabolism. *64*, 105–113. 10.1016/j.metabol.2014.10.021.

61. Reid, I.R., Baldock, P.A., and Cornish, J. (2018). Effects of Leptin on the Skeleton. Endocr. Rev. *39*, 938–959. 10.1210/er.2017-00226.

62. Kishida, Y., Hirao, M., Tamai, N., Nampei, A., Fujimoto, T., Nakase, T., Shimizu, N., Yoshikawa, H., and Myoui, A. (2005). Leptin regulates chondrocyte differentiation and matrix maturation during endochondral ossification. Bone *37*, 607–621. 10.1016/j.bone.2005.05.009.

63. Cheng, M., Li, T., Li, W., Chen, Y., Xu, W., and Xu, L. (2018). Leptin can promote mineralization and up-regulate RANKL mRNA expression in osteoblasts from adult female SD rats. Int. J. Clin. Exp. Pathol. *11*, 1610–1619.

64. Ducy, P., Amling, M., Takeda, S., Priemel, M., Schilling, A.F., Beil, F.T., Shen, J., Vinson, C., Rueger, J.M., and Karsenty, G. (2000). Leptin inhibits bone formation through a hypothalamic relay: a central control of bone mass. Cell *100*, 197–207. 10.1016/s0092-8674(00)81558-5.

65. Karsenty, G., and Khosla, S. (2022). The crosstalk between bone remodeling and energy metabolism: A translational perspective. Cell Metab. *34*, 805–817. 10.1016/j.cmet.2022.04.010.

66. Ealey, K.N., Fonseca, D., Archer, M.C., and Ward, W.E. (2006). Bone abnormalities in adolescent leptin-deficient mice. Regul. Pept. *136*, 9–13. 10.1016/j.regpep.2006.04.013.

67. Hamrick, M.W., Della-Fera, M.A., Choi, Y.-H., Pennington, C., Hartzell, D., and Baile, C.A. (2005). Leptin treatment induces loss of bone marrow adipocytes and increases bone formation in leptin-deficient ob/ob mice. J. Bone Miner. Res. Off. J. Am. Soc. Bone Miner. Res. *20*, 994–1001. 10.1359/JBMR.050103.

68. Hamrick, M.W., Pennington, C., Newton, D., Xie, D., and Isales, C. (2004). Leptin deficiency produces contrasting phenotypes in bones of the limb and spine. Bone *34*, 376–383. 10.1016/j.bone.2003.11.020.

69. Bodosi, B., Gardi, J., Hajdu, I., Szentirmai, E., Obal, F., and Krueger, J.M. (2004). Rhythms of ghrelin, leptin, and sleep in rats: effects of the normal diurnal cycle, restricted feeding, and sleep deprivation. Am. J. Physiol. Regul. Integr. Comp. Physiol. *287*, R1071-1079. 10.1152/ajpregu.00294.2004.

70. Templeman, I., Smith, H.A., Walhin, J.-P., Middleton, B., Gonzalez, J.T., Karagounis, L.G., Johnston, J.D., and Betts, J.A. (2021). Unacylated ghrelin, leptin, and appetite display diurnal rhythmicity in lean adults. J. Appl. Physiol. Bethesda Md 1985 *130*, 1534–1543. 10.1152/japplphysiol.00920.2020.

71. Shrestha, A., Müllner, E., Poutanen, K., Mykkänen, H., and Moazzami, A.A. (2017). Metabolic changes in serum metabolome in response to a meal. Eur. J. Nutr. *56*, 671–681. 10.1007/s00394-015-1111-y.

72. Dallmann, R., Viola, A.U., Tarokh, L., Cajochen, C., and Brown, S.A. (2012). The human circadian metabolome. Proc. Natl. Acad. Sci. *109*, 2625–2629. 10.1073/pnas.1114410109.

73. Buijs, R., Salgado, R., Sabath, E., and Escobar, C. (2013). Peripheral circadian oscillators: time and food. Prog. Mol. Biol. Transl. Sci. *119*, 83–103. 10.1016/B978-0-12-396971-2.00004-X.

74. Challet, E. (2013). Circadian clocks, food intake, and metabolism. Prog. Mol. Biol. Transl. Sci. *119*, 105–135. 10.1016/B978-0-12-396971-2.00005-1.

75. Eckel-Mahan, K., and Sassone-Corsi, P. (2013). Metabolism and the circadian clock converge. Physiol. Rev. *93*, 107–135. 10.1152/physrev.00016.2012.

76. Christou, S., Wehrens, S.M.T., Isherwood, C., Möller-Levet, C.S., Wu, H., Revell, V.L., Bucca, G., Skene, D.J., Laing, E.E., Archer, S.N., et al. (2019). Circadian regulation in human white adipose tissue revealed by transcriptome and metabolic network analysis. Sci. Rep. *9*, 2641. 10.1038/s41598-019-39668-3.

77. Loboda, A., Kraft, W.K., Fine, B., Joseph, J., Nebozhyn, M., Zhang, C., He, Y., Yang, X., Wright, C., Morris, M., et al. (2009). Diurnal variation of the human adipose transcriptome and the link to metabolic disease. BMC Med. Genomics *2*, 7. 10.1186/1755-8794-2-7.

78. Stenvers, D.J., Jongejan, A., Atiqi, S., Vreijling, J.P., Limonard, E.J., Endert, E., Baas, F., Moerland, P.D., Fliers, E., Kalsbeek, A., et al. (2019). Diurnal rhythms in the white adipose tissue transcriptome are disturbed in obese individuals with type 2 diabetes compared with lean control individuals. Diabetologia *62*, 704–716. 10.1007/s00125-019-4813-5.

79. Zvonic, S., Ptitsyn, A.A., Conrad, S.A., Scott, L.K., Floyd, Z.E., Kilroy, G., Wu, X., Goh, B.C., Mynatt, R.L., and Gimble, J.M. (2006). Characterization of peripheral circadian clocks in adipose tissues. Diabetes *55*, 962–970. 10.2337/diabetes.55.04.06.db05-0873.

80. Ceglia, N., Liu, Y., Chen, S., Agostinelli, F., Eckel-Mahan, K., Sassone-Corsi, P., and Baldi, P. (2018). CircadiOmics: circadian omic web portal. Nucleic Acids Res. *46*, W157–W162. 10.1093/nar/gky441.

81. Hu, J., Li, T., Du, S., Chen, Y., Wang, S., Xiong, F., and Wu, Q. (2015). The MAPK signaling pathway mediates the GPR91-dependent release of VEGF from RGC-5 cells. Int. J. Mol. Med. *36*, 130–138. 10.3892/ijmm.2015.2195.

82. Trefts, E., and Shaw, R.J. (2021). AMPK: restoring metabolic homeostasis over space and time. Mol. Cell *81*, 3677–3690. 10.1016/j.molcel.2021.08.015.

83. Daval, M., Diot-Dupuy, F., Bazin, R., Hainault, I., Viollet, B., Vaulont, S., Hajduch, E., Ferré, P., and Foufelle, F. (2005). Anti-lipolytic action of AMP-activated protein kinase in rodent adipocytes. J. Biol. Chem. *280*, 25250–25257. 10.1074/jbc.M414222200.

84. Sponarova, J., Mustard, K.J., Horakova, O., Flachs, P., Rossmeisl, M., Brauner, P., Bardova, K., Thomason-Hughes, M., Braunerova, R., Janovska, P., et al. (2005). Involvement of AMP-activated protein kinase in fat depot-specific metabolic changes during starvation. FEBS Lett. *579*, 6105–6110. 10.1016/j.febslet.2005.09.078.

85. Park, H., Kaushik, V.K., Constant, S., Prentki, M., Przybytkowski, E., Ruderman, N.B., and Saha, A.K. (2002). Coordinate regulation of malonyl-CoA decarboxylase, sn-glycerol-3-

phosphate acyltransferase, and acetyl-CoA carboxylase by AMP-activated protein kinase in rat tissues in response to exercise. J. Biol. Chem. *277*, 32571–32577. 10.1074/jbc.M201692200.

86. Musi, N., Hayashi, T., Fujii, N., Hirshman, M.F., Witters, L.A., and Goodyear, L.J. (2001). AMP-activated protein kinase activity and glucose uptake in rat skeletal muscle. Am. J. Physiol. Endocrinol. Metab. *280*, E677-684. 10.1152/ajpendo.2001.280.5.E677.

87. Salt, I.P., Connell, J.M., and Gould, G.W. (2000). 5-aminoimidazole-4-carboxamide ribonucleoside (AICAR) inhibits insulin-stimulated glucose transport in 3T3-L1 adipocytes. Diabetes *49*, 1649–1656. 10.2337/diabetes.49.10.1649.

88. Sakoda, H., Ogihara, T., Anai, M., Fujishiro, M., Ono, H., Onishi, Y., Katagiri, H., Abe, M., Fukushima, Y., Shojima, N., et al. (2002). Activation of AMPK is essential for AICAR-induced glucose uptake by skeletal muscle but not adipocytes. Am. J. Physiol. Endocrinol. Metab. *282*, E1239-1244. 10.1152/ajpendo.00455.2001.

89. Chuang, S.-J., Johanns, M., Pyr Dit Ruys, S., Steinberg, G.R., Kemp, B.E., Viollet, B., and Rider, M.H. (2021). AMPK activation by SC4 inhibits noradrenaline-induced lipolysis and insulin-stimulated lipogenesis in white adipose tissue. Biochem. J. *478*, 3869–3889. 10.1042/BCJ20210411.

90. Szkudelski, T., and Szkudelska, K. (2017). Effects of AMPK activation on lipolysis in primary rat adipocytes: studies at different glucose concentrations. Arch. Physiol. Biochem. *123*, 43–49. 10.1080/13813455.2016.1227853.

91. Lihn, A.S., Jessen, N., Pedersen, S.B., Lund, S., and Richelsen, B. (2004). AICAR stimulates adiponectin and inhibits cytokines in adipose tissue. Biochem. Biophys. Res. Commun. *316*, 853–858. 10.1016/j.bbrc.2004.02.139.

92. Sell, H., Dietze-Schroeder, D., Eckardt, K., and Eckel, J. (2006). Cytokine secretion by human adipocytes is differentially regulated by adiponectin, AICAR, and troglitazone. Biochem. Biophys. Res. Commun. *343*, 700–706. 10.1016/j.bbrc.2006.03.010.

93. Wu, X., Motoshima, H., Mahadev, K., Stalker, T.J., Scalia, R., and Goldstein, B.J. (2003). Involvement of AMP-activated protein kinase in glucose uptake stimulated by the globular domain of adiponectin in primary rat adipocytes. Diabetes *52*, 1355–1363. 10.2337/diabetes.52.6.1355.

94. Orci, L., Cook, W.S., Ravazzola, M., Wang, M.-Y., Park, B.-H., Montesano, R., and Unger, R.H. (2004). Rapid transformation of white adipocytes into fat-oxidizing machines. Proc. Natl. Acad. Sci. U. S. A. *101*, 2058–2063. 10.1073/pnas.0308258100.

95. Jordan, S.D., and Lamia, K.A. (2013). AMPK at the crossroads of circadian clocks and metabolism. Mol. Cell. Endocrinol. *366*, 163–169. 10.1016/j.mce.2012.06.017.

96. Um, J.H., Yang, S., Yamazaki, S., Kang, H., Viollet, B., Foretz, M., and Chung, J.H. (2007). Activation of 5'-AMP-activated kinase with diabetes drug metformin induces casein kinase Iepsilon (CKIepsilon)-dependent degradation of clock protein mPer2. J. Biol. Chem. *282*, 20794–20798. 10.1074/jbc.C700070200.

97. Lamia, K.A., Sachdeva, U.M., DiTacchio, L., Williams, E.C., Alvarez, J.G., Egan, D.F., Vasquez, D.S., Juguilon, H., Panda, S., Shaw, R.J., et al. (2009). AMPK regulates the circadian clock by cryptochrome phosphorylation and degradation. Science *326*, 437–440. 10.1126/science.1172156.

98. Trauelsen, M., Hiron, T.K., Lin, D., Petersen, J.E., Breton, B., Husted, A.S., Hjorth, S.A., Inoue, A., Frimurer, T.M., Bouvier, M., et al. (2021). Extracellular succinate hyperpolarizes M2 macrophages through SUCNR1/GPR91-mediated Gq signaling. Cell Rep. *35*, 109246. 10.1016/j.celrep.2021.109246.

99. World Health Organization (2000). Obesity: preventing and managing the global epidemic. Report of a WHO consultation. World Health Organ. Tech. Rep. Ser. *894*, i–xii, 1–253.

100. Calvo, E., Keiran, N., Núñez-Roa, C., Maymó-Masip, E., Ejarque, M., Sabadell-Basallote, J., Del Mar Rodríguez-Peña, M., Ceperuelo-Mallafré, V., Seco, J., Benaiges, E., et al. (2021). Effects of stem cells from inducible brown adipose tissue on diet-induced obesity in mice. Sci. Rep. *11*, 13923. 10.1038/s41598-021-93224-6.

101. Pachón-Peña, G., Yu, G., Tucker, A., Wu, X., Vendrell, J., Bunnell, B.A., and Gimble, J.M. (2011). Stromal stem cells from adipose tissue and bone marrow of age-matched female donors display distinct immunophenotypic profiles. J. Cell. Physiol. *226*, 843–851. 10.1002/jcp.22408.

102. Del Río-Martín, A., Pérez-Taboada, I., Fernández-Pérez, A., Moratalla, R., de la Villa, P., and Vallejo, M. (2019). Hypomorphic Expression of Pitx3 Disrupts Circadian Clocks and Prevents Metabolic Entrainment of Energy Expenditure. Cell Rep. *29*, 3678-3692.e4. 10.1016/j.celrep.2019.11.027.

103. Tang, H., Vasselli, J.R., Wu, E.X., Boozer, C.N., and Gallagher, D. (2002). High-resolution magnetic resonance imaging tracks changes in organ and tissue mass in obese and aging rats. Am. J. Physiol. Regul. Integr. Comp. Physiol. *282*, R890-899. 10.1152/ajpregu.0527.2001.

104. Estañ, M.C., Fernández-Núñez, E., Zaki, M.S., Esteban, M.I., Donkervoort, S., Hawkins, C., Caparros-Martin, J.A., Saade, D., Hu, Y., Bolduc, V., et al. (2019). Recessive mutations in muscle-specific isoforms of FXR1 cause congenital multi-minicore myopathy. Nat. Commun. *10*, 797. 10.1038/s41467-019-08548-9.

105. Dobin, A., Davis, C.A., Schlesinger, F., Drenkow, J., Zaleski, C., Jha, S., Batut, P., Chaisson, M., and Gingeras, T.R. (2013). STAR: ultrafast universal RNA-seq aligner. Bioinforma. Oxf. Engl. *29*, 15–21. 10.1093/bioinformatics/bts635.

106. Liao, Y., Smyth, G.K., and Shi, W. (2019). The R package Rsubread is easier, faster, cheaper and better for alignment and quantification of RNA sequencing reads. Nucleic Acids Res. *47*, e47. 10.1093/nar/gkz114.

107. Yeom, M., Pendergast, J.S., Ohmiya, Y., and Yamazaki, S. (2010). Circadian-independent cell mitosis in immortalized fibroblasts. Proc. Natl. Acad. Sci. U. S. A. *107*, 9665–9670. 10.1073/pnas.0914078107.

108. Mina, A.I., LeClair, R.A., LeClair, K.B., Cohen, D.E., Lantier, L., and Banks, A.S. (2018). CalR: A Web-Based Analysis Tool for Indirect Calorimetry Experiments. Cell Metab. *28*, 656-666.e1. 10.1016/j.cmet.2018.06.019.

109. R Core Team (2022). R: A language and environment for statistical computing. R Foundation for Statistical Computing, Viena, Austria. Available online at https://www.R-project.org/.

110. Wickham, H. (2016). ggplot2: Elegant Graphics for Data Analysis (Springer-Verlag New York).

111. Ritchie, M.E., Phipson, B., Wu, D., Hu, Y., Law, C.W., Shi, W., and Smyth, G.K. (2015). limma powers differential expression analyses for RNA-sequencing and microarray studies. Nucleic Acids Res. *43*, e47. 10.1093/nar/gkv007.

112. Love, M.I., Huber, W., and Anders, S. (2014). Moderated estimation of fold change and dispersion for RNA-seq data with DESeq2. Genome Biol. *15*, 550. 10.1186/s13059-014-0550-8.

113. Wu, D., Lim, E., Vaillant, F., Asselin-Labat, M.-L., Visvader, J.E., and Smyth, G.K. (2010). ROAST: rotation gene set tests for complex microarray experiments. Bioinforma. Oxf. Engl. *26*, 2176–2182. 10.1093/bioinformatics/btq401.

114. Efron, B., and Tibshirani, R. (2007). On Testing the Significance of Sets of Genes. Ann. Appl. Stat. *1*, 107–129.

115. Carlson, M. (2019). org.Hs.eg.db: Genome wide annotation for Human. R package version 2.14.0.

HIGHLIGHTS

1- Extracellular succinate in adipocytes controls circadian clock and leptin via SUCNR1

2- SUCNR1 modulates leptin via AMPK/JNK-BMAL1-C/EBP/α-dependent signaling

3- The metabolic impact of SUCNR1 deficiency in adipocytes is dependent on nutritional status

4- Hyperleptinemia in human obesity is related to overactive succinate/SUCNR1 signaling

eTOC blurb

Villanueva-Carmona et al. describe a new function for the succinate/SUCNR1 axis in controlling leptin expression in adipocytes via a mechanism involving the circadian clock. This system is overactivated in obesity, which might contribute to obesity-related hyperleptinemia.

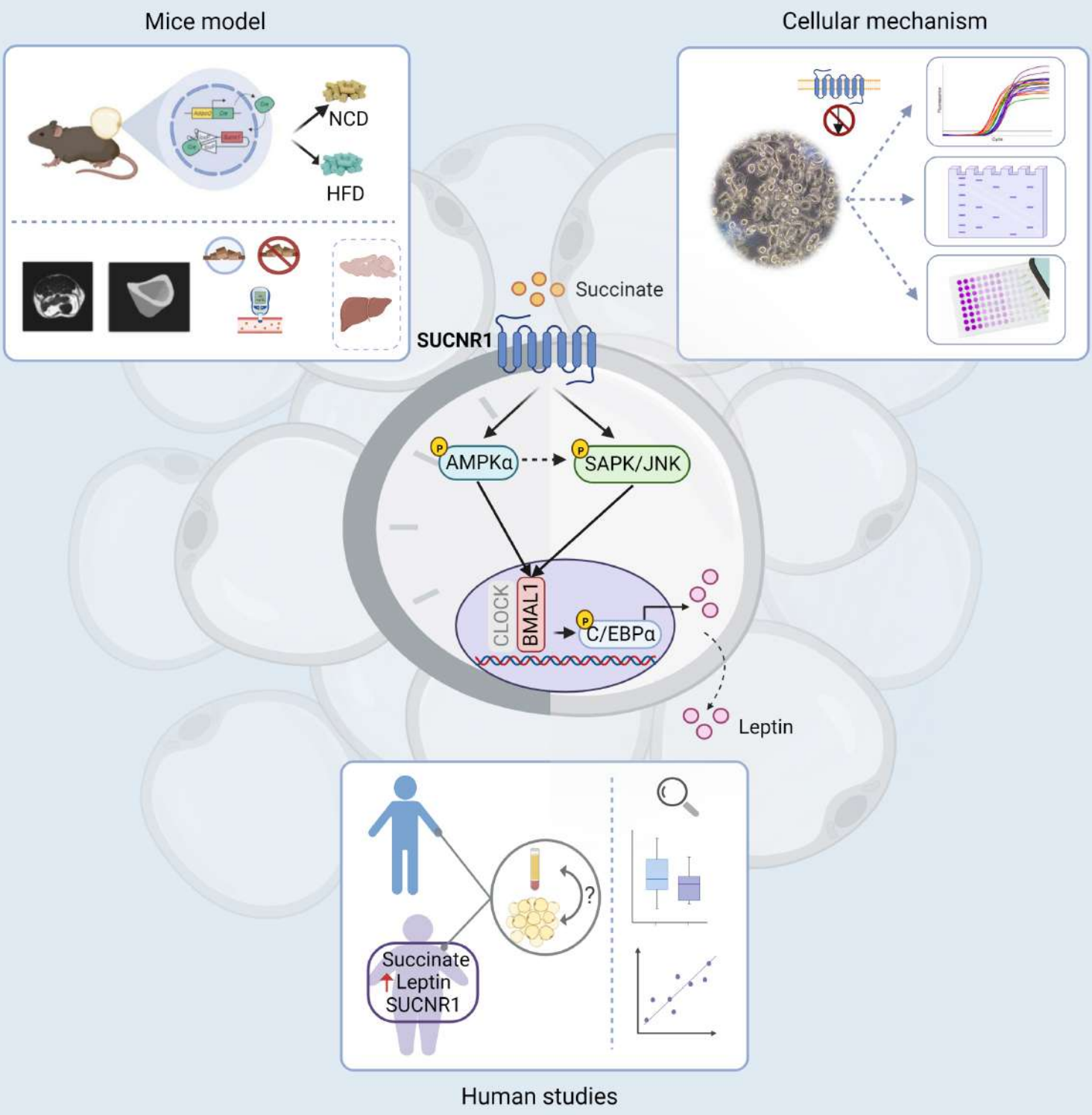
Mice model
NCD
HFD
Cellular mechanism
Succinate
SUCNR1
AMPKα
SAPK/JNK
CLOCK
BMAL1
C/EBPα
Leptin
Succinate
Leptin
SUCNR1
?
Human studies

Figure 1

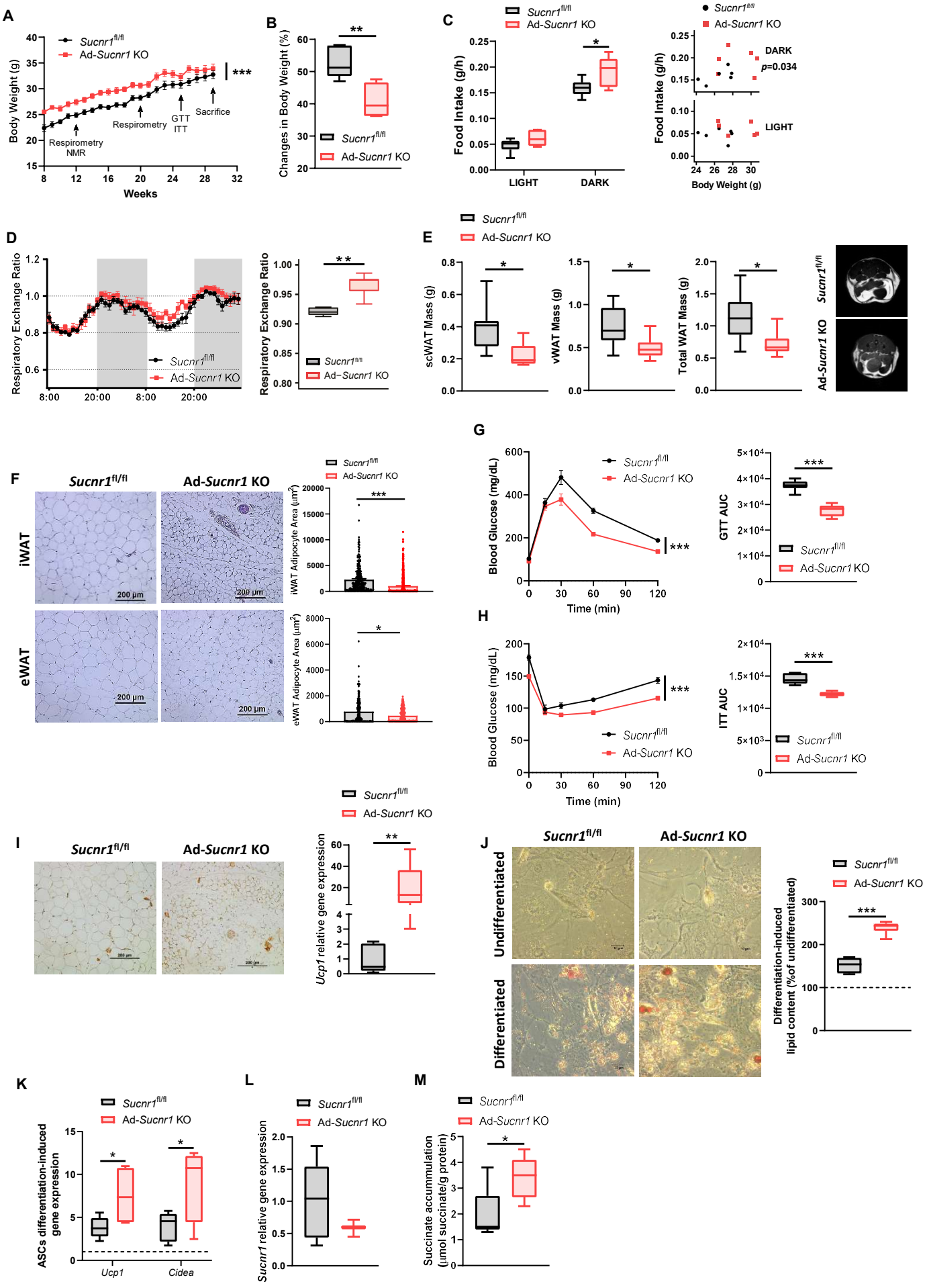
A
Body Weight (g)
Weeks
Sucnr1fl/fl
Ad-Sucnr1 KO
***
Respirometry NMR
Respirometry
GTT ITT
Sacrifice
B
Changes in Body Weight (%)
**
C
Food Intake (g/h)
LIGHT
DARK
*
DARK
p=0.034
LIGHT
Body Weight (g)
D
Respiratory Exchange Ratio
8:00
20:00
E
scWAT Mass (g)
vWAT Mass (g)
Total WAT Mass (g)
F
Sucnr1fl/fl
Ad-Sucnr1 KO
iWAT
eWAT
200 µm
iWAT Adipocyte Area (µm2)
eWAT Adipocyte Area (µm2)
G
Blood Glucose (mg/dL)
Time (min)
GTT AUC
H
ITT AUC
I
Ucp1 relative gene expression
J
Undifferentiated
Differentiated
Differentiation-induced lipid content (%of undifferentiated)
K
ASCs differentiation-induced gene expression
Ucp1
Cidea
L
Sucnr1 relative gene expression
M
Succinate accummulation (µmol succinate/g protein)

Figure 2

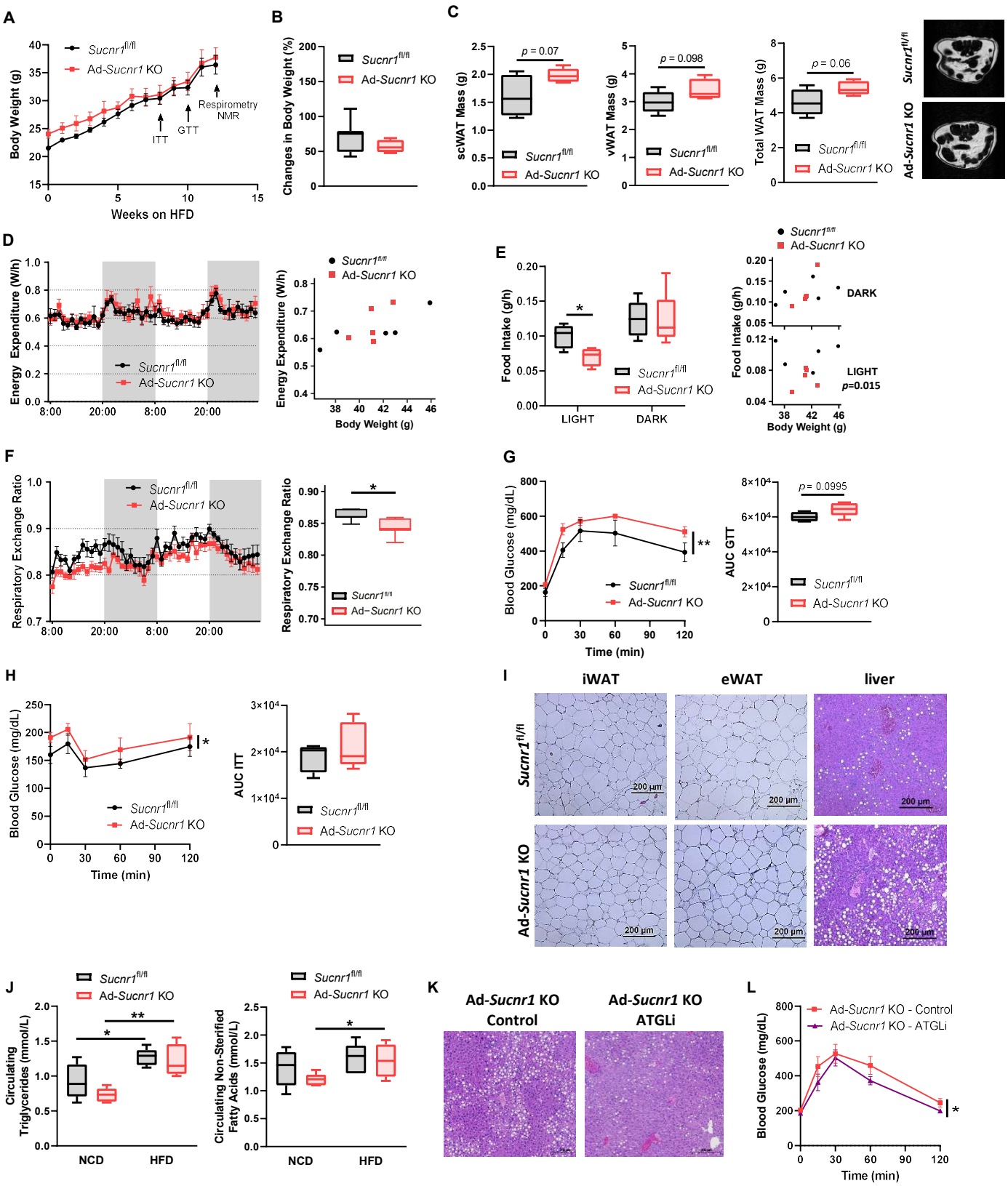
A
Body Weight (g)
Weeks on HFD
Sucnr1fl/fl
Ad-Sucnr1 KO
ITT
GTT
Respirometry NMR
B
Changes in Body Weight (%)
C
scWAT Mass (g)
vWAT Mass (g)
Total WAT Mass (g)
p = 0.07
p = 0.098
p = 0.06
Sucnr1fl/fl
Ad-Sucnr1 KO
D
Energy Expenditure (W/h)
Body Weight (g)
E
Food Intake (g/h)
LIGHT
DARK
p=0.015
F
Respiratory Exchange Ratio
G
Blood Glucose (mg/dL)
Time (min)
AUC GTT
p= 0.0995
H
AUC ITT
I
iWAT
eWAT
liver
200 µm
J
Circulating Triglycerides (mmol/L)
Circulating Non-Sterified Fatty Acids (mmol/L)
NCD
HFD
K
Ad-Sucnr1 KO Control
Ad-Sucnr1 KO ATGLi
L
Ad-Sucnr1 KO - Control
Ad-Sucnr1 KO - ATGLi

Figure 3

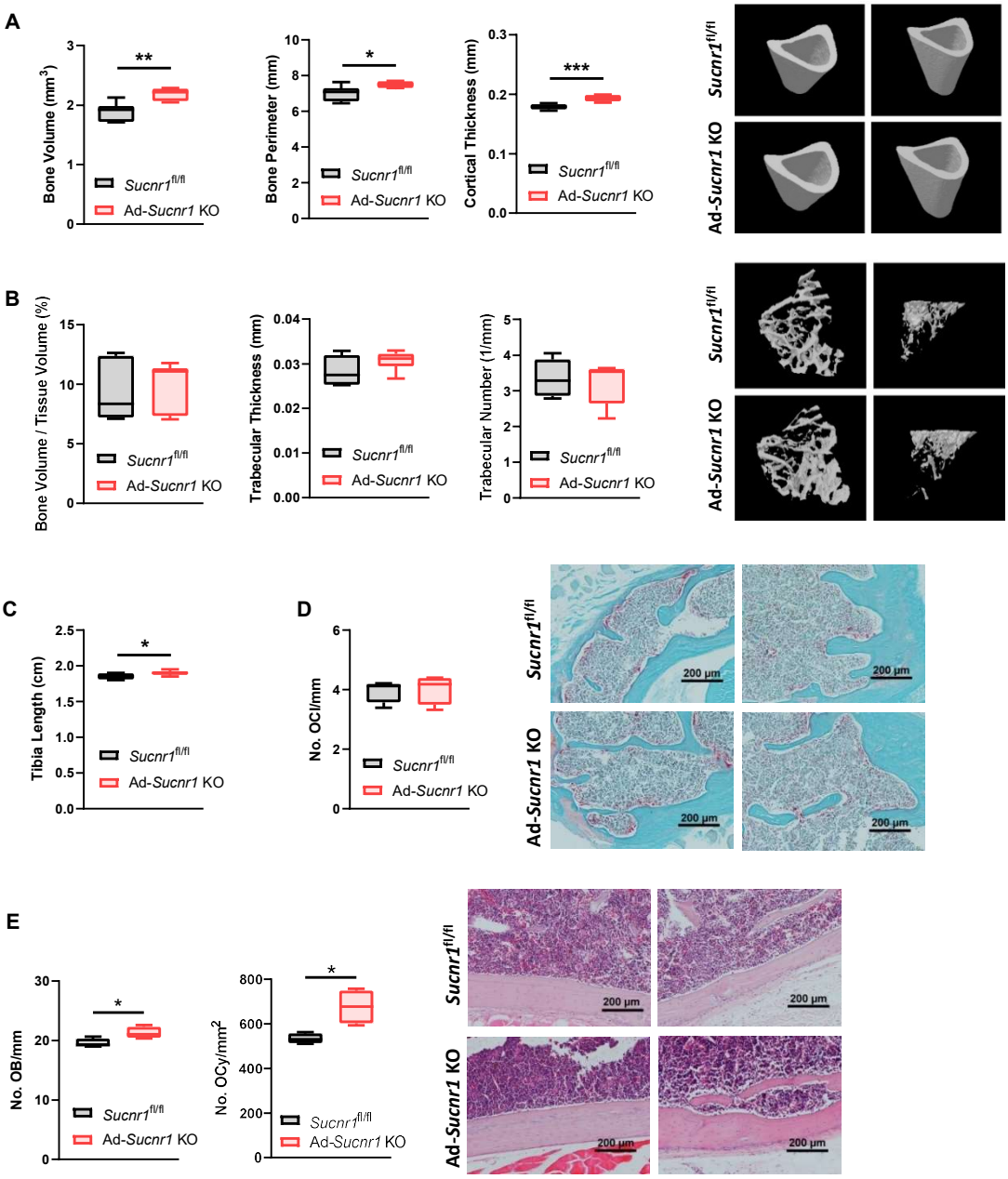
A
Bone Volume (mm3)
Bone Perimeter (mm)
Cortical Thickness (mm)
Sucnr1fl/fl
Ad-Sucnr1 KO
B
Bone Volume / Tissue Volume (%)
Trabecular Thickness (mm)
Trabecular Number (1/mm)
C
Tibia Length (cm)
D
No. OCl/mm
200 µm
E
No. OB/mm
No. OCy/mm2

Figure 4

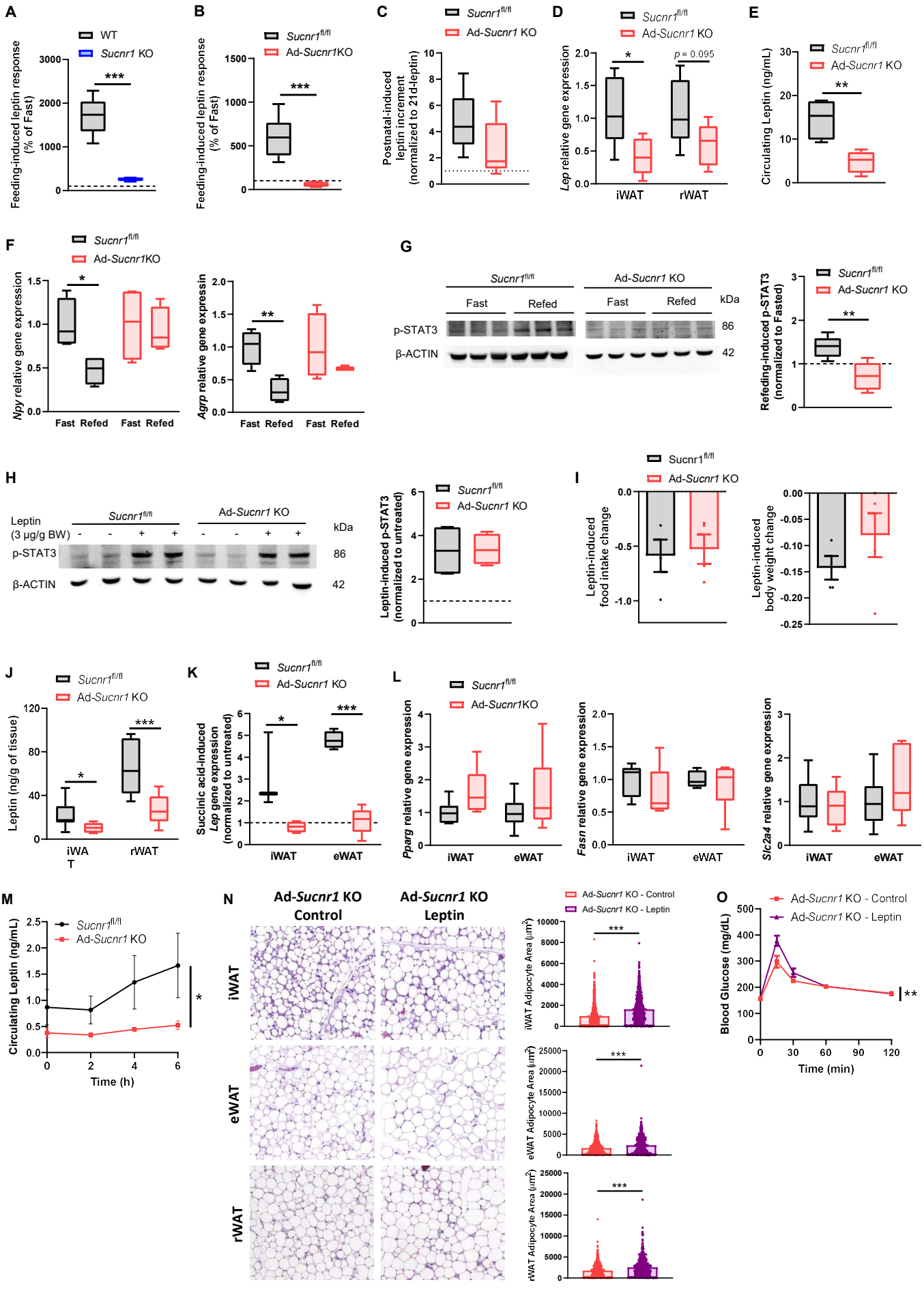
A
WT
Sucnr1 KO
Feeding-induced leptin response (% of Fast)
***
B
Sucnr1fl/fl
Ad-Sucnr1KO
Feeding-induced leptin response (% of Fast)
***
C
Sucnr1fl/fl
Ad-Sucnr1 KO
Postnatal-induced leptin increment (normalized to 21d-leptin)
D
Sucnr1fl/fl
Ad-Sucnr1 KO
Lep relative gene expression
*
p = 0.095
iWAT
rWAT
E
Sucnr1fl/fl
Ad-Sucnr1 KO
Circulating Leptin (ng/mL)
**
F
Sucnr1fl/fl
Ad-Sucnr1KO
Npy relative gene expression
*
Fast Refed Fast Refed
Agrp relative gene expressin
**
Fast Refed Fast Refed
G
Sucnr1fl/fl
Ad-Sucnr1 KO
Fast
Refed
Fast
Refed
kDa
p-STAT3
86
β-ACTIN
42
Refeding-induced p-STAT3 (normalized to Fasted)
**
H
Leptin (3 μg/g BW)
Sucnr1fl/fl
Ad-Sucnr1 KO
kDa
p-STAT3
86
β-ACTIN
42
Leptin-induced p-STAT3 (normalized to untreated)
I
Sucnr1fl/fl
Ad-Sucnr1 KO
Leptin-induced food intake change
Leptin-induced body weight change
J
Sucnr1fl/fl
Ad-Sucnr1 KO
Leptin (ng/g of tissue)
*
***
iWAT
rWAT
K
Sucnr1fl/fl
Ad-Sucnr1 KO
Succinic acid-induced Lep gene expression (normalized to untreated)
*
***
iWAT
eWAT
L
Sucnr1fl/fl
Ad-Sucnr1KO
Pparg relative gene expression
Fasn relative gene expression
Slc2a4 relative gene expression
iWAT
eWAT
M
Sucnr1fl/fl
Ad-Sucnr1 KO
Circulating Leptin (ng/mL)
*
Time (h)
N
Ad-Sucnr1 KO Control
Ad-Sucnr1 KO Leptin
Ad-Sucnr1 KO - Control
Ad-Sucnr1 KO - Leptin
iWAT
eWAT
rWAT
iWAT Adipocyte Area (μm2)
eWAT Adipocyte Area (μm2)
rWAT Adipocyte Area (μm2)
***
O
Ad-Sucnr1 KO - Control
Ad-Sucnr1 KO - Leptin
Blood Glucose (mg/dL)
**
Time (min)

Figure 5

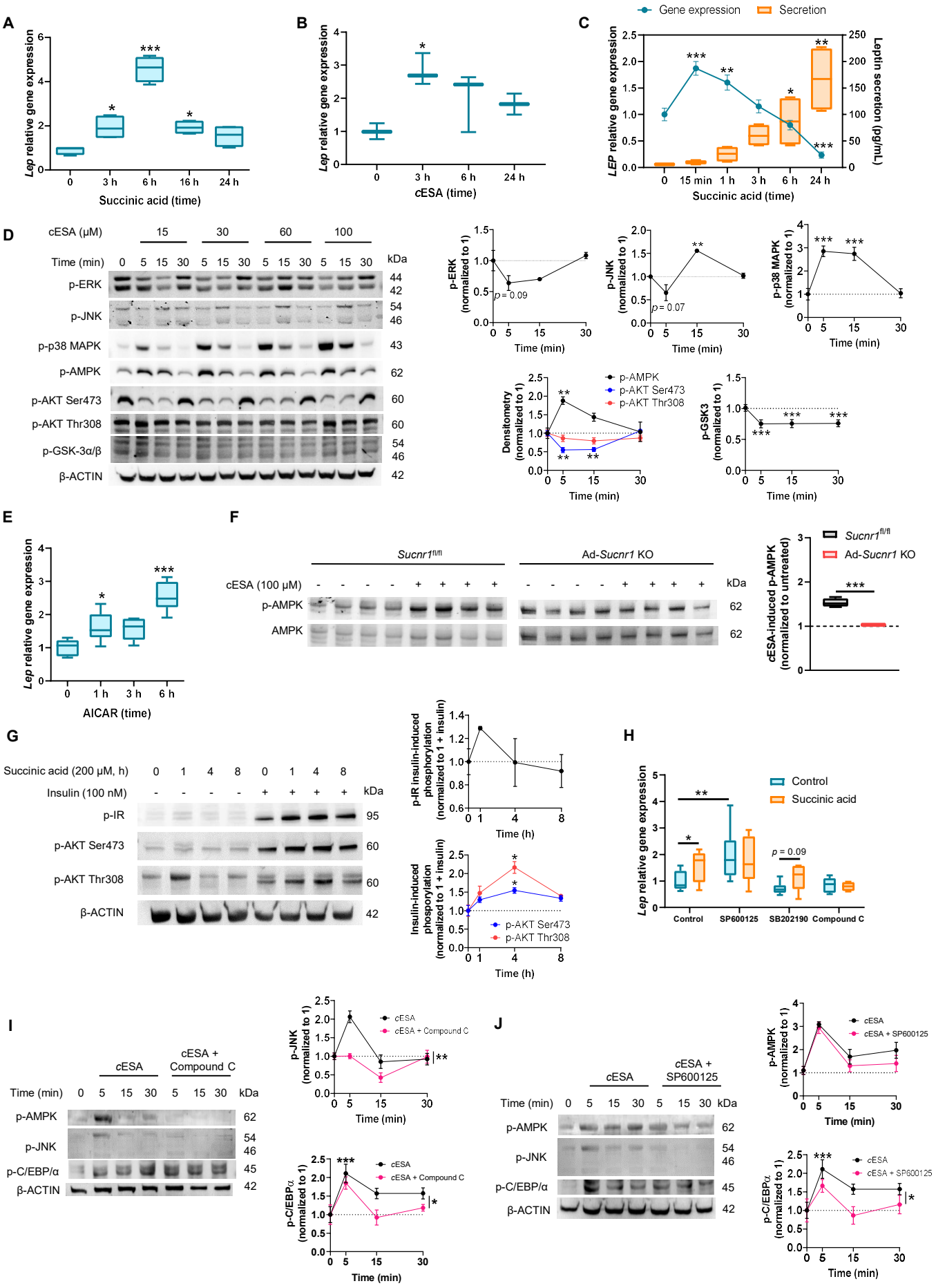
A
Lep relative gene expression
Succinic acid (time)
0
3 h
6 h
16 h
24 h
B
Lep relative gene expression
cESA (time)
C
Gene expression
Secretion
LEP relative gene expression
Leptin secretion (pg/mL)
Succinic acid (time)
D
cESA (μM)
Time (min)
kDa
p-ERK
p-JNK
p-p38 MAPK
p-AMPK
p-AKT Ser473
p-AKT Thr308
p-GSK-3α/β
β-ACTIN
p-ERK (normalized to 1)
p-JNK (normalized to 1)
p-p38 MAPK (normalized to 1)
Densitometry (normalized to 1)
p-GSK3 (normalized to 1)
Time (min)
E
Lep relative gene expression
AICAR (time)
F
Sucnr1fl/fl
Ad-Sucnr1 KO
cESA (100 μM)
p-AMPK
AMPK
cESA-induced p-AMPK (normalized to untreated)
G
Succinic acid (200 μM, h)
Insulin (100 nM)
p-IR
p-AKT Ser473
p-AKT Thr308
β-ACTIN
p-IR insulin-induced phosphorylation (normalized to 1 + insulin)
Insulin-induced phosporylation (normalized to 1 + insulin)
Time (h)
H
Lep relative gene expression
Control
Succinic acid
Control
SP600125
SB202190
Compound C
I
cESA
cESA + Compound C
p-AMPK
p-JNK
p-C/EBPα
β-ACTIN
p-JNK (normalized to 1)
p-C/EBPα (normalized to 1)
J
cESA
cESA + SP600125
p-AMPK (normalized to 1)
p-C/EBPα (normalized to 1)

Figure 6

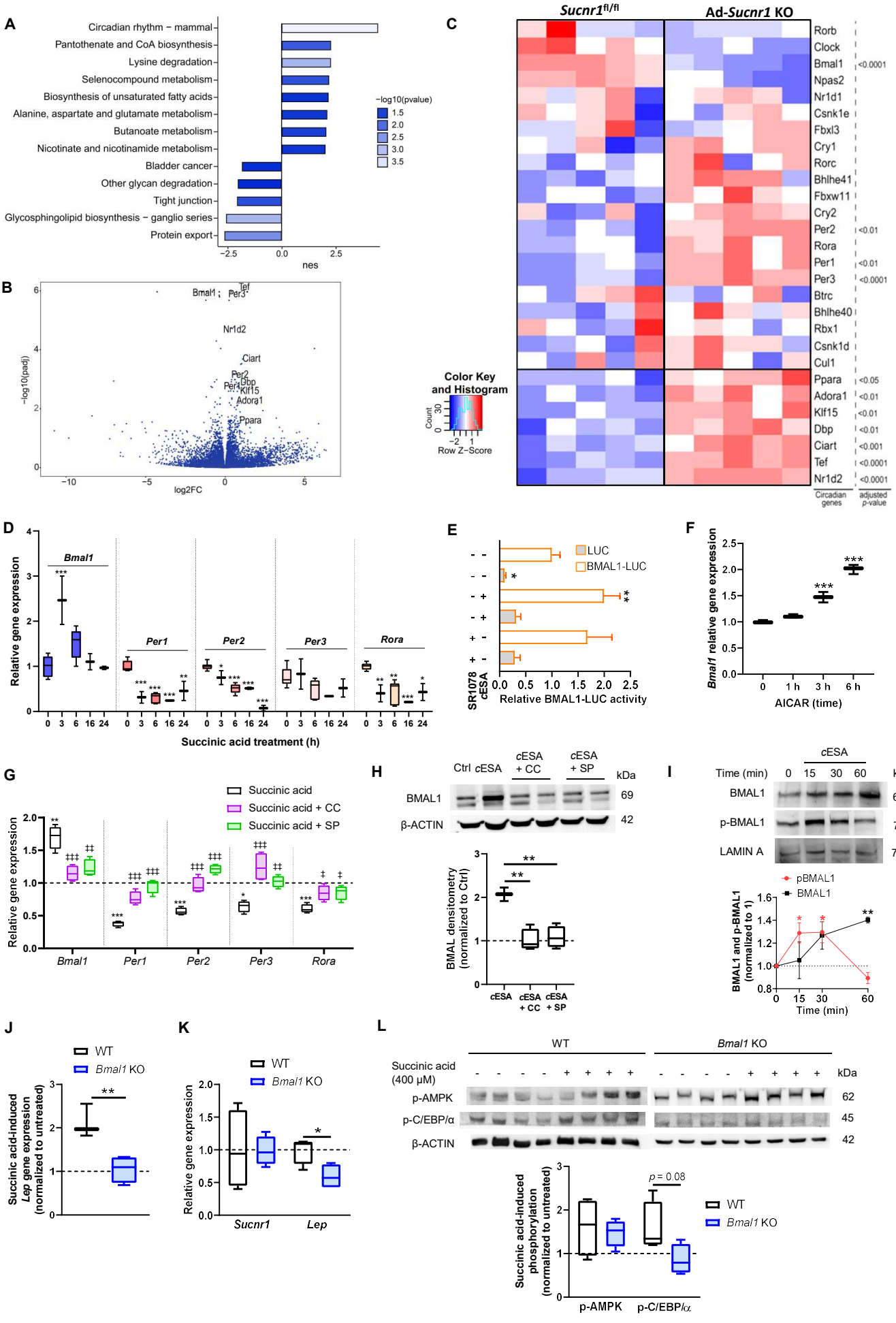
A
Circadian rhythm − mammal
Pantothenate and CoA biosynthesis
Lysine degradation
Selenocompound metabolism
Biosynthesis of unsaturated fatty acids
Alanine, aspartate and glutamate metabolism
Butanoate metabolism
Nicotinate and nicotinamide metabolism
Bladder cancer
Other glycan degradation
Tight junction
Glycosphingolipid biosynthesis − ganglio series
Protein export
−log10(pvalue)
1.5
2.0
2.5
3.0
3.5
−2.5
0.0
2.5
nes
B
Bmal1
Tef
Per3
Nr1d2
Ciart
Per2
Dbp
Per1
Klf15
Adora1
Ppara
−log10(padj)
log2FC
C
Sucnr1fl/fl
Ad-Sucnr1 KO
Color Key and Histogram
Count
Row Z−Score
Rorb
Clock
Bmal1
Npas2
Nr1d1
Csnk1e
Fbxl3
Cry1
Rorc
Bhlhe41
Fbxw11
Cry2
Per2
Rora
Per1
Per3
Btrc
Bhlhe40
Rbx1
Csnk1d
Cul1
Ppara
Adora1
Klf15
Dbp
Ciart
Tef
Nr1d2
<0.0001
<0.01
<0.05
<0.001
Circadian genes
adjusted p-value
D
Bmal1
Per1
Per2
Per3
Rora
Relative gene expression
Succinic acid treatment (h)
E
LUC
BMAL1-LUC
SR1078
cESA
Relative BMAL1-LUC activity
F
Bmal1 relative gene expression
AICAR (time)
G
Succinic acid
Succinic acid + CC
Succinic acid + SP
Relative gene expression
H
Ctrl
cESA
cESA + CC
cESA + SP
kDa
BMAL1
β-ACTIN
69
42
BMAL densitometry (normalized to Ctrl)
I
Time (min)
cESA
BMAL1
p-BMAL1
LAMIN A
78
70
BMAL1 and p-BMAL1 (normalized to 1)
J
WT
Bmal1 KO
Succinic acid-induced Lep gene expression (normalized to untreated)
K
Sucnr1
Lep
L
Succinic acid (400 μM)
p-AMPK
p-C/EBPα
62
45
p = 0.08
Succinic acid-induced phosphorylation (normalized to untreated)

Figure 7

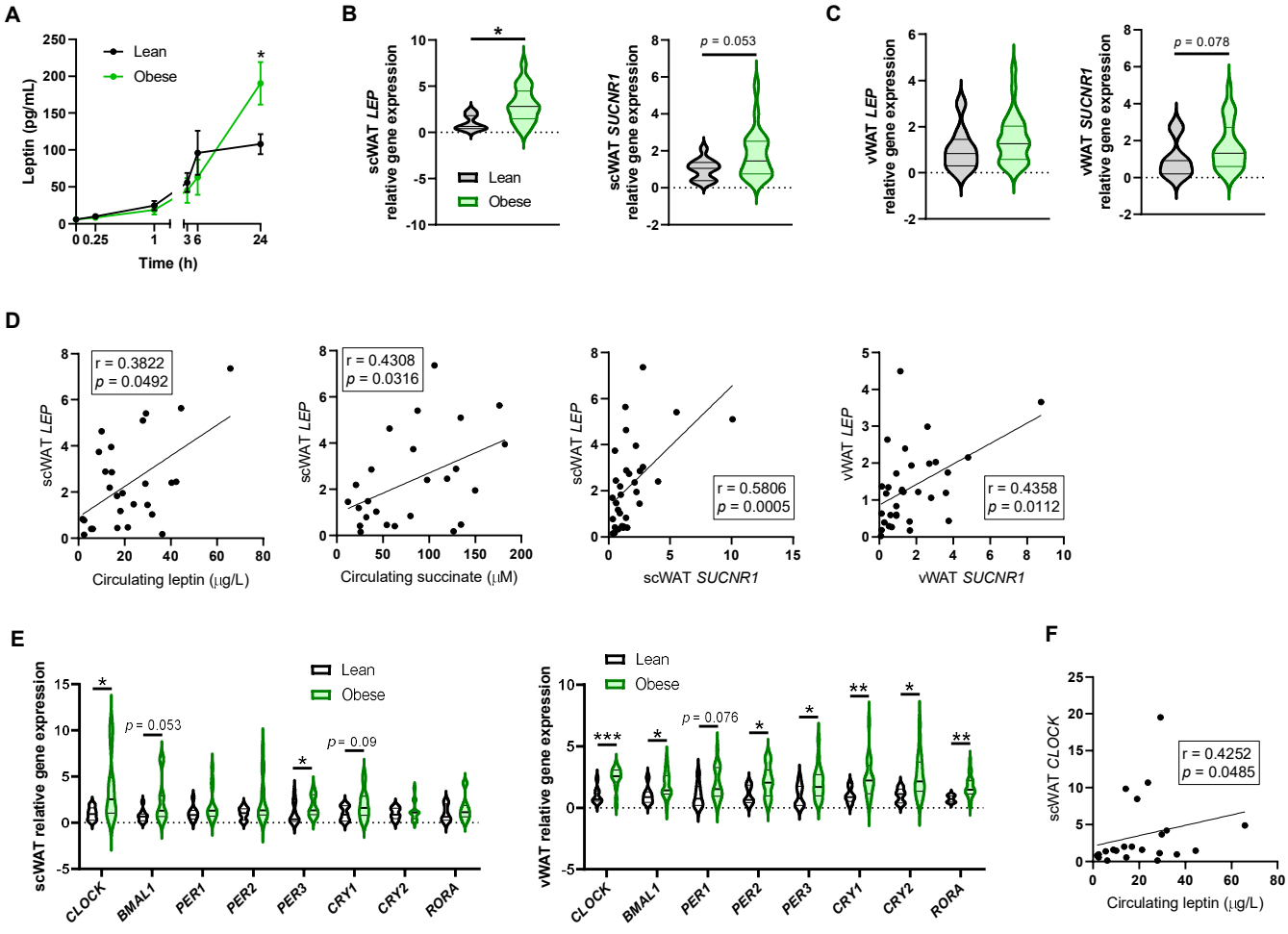
A
Leptin (pg/mL)
Lean
Obese
Time (h)
B
scWAT LEP relative gene expression
scWAT SUCNR1 relative gene expression
p = 0.053
C
vWAT LEP relative gene expression
vWAT SUCNR1 relative gene expression
p = 0.078
D
scWAT LEP
r = 0.3822
p = 0.0492
Circulating leptin (µg/L)
r = 0.4308
p = 0.0316
Circulating succinate (µM)
r = 0.5806
p = 0.0005
scWAT SUCNR1
vWAT LEP
r = 0.4358
p = 0.0112
vWAT SUCNR1
E
scWAT relative gene expression
vWAT relative gene expression
p = 0.053
p = 0.09
p = 0.076
CLOCK
BMAL1
PER1
PER2
PER3
CRY1
CRY2
RORA
F
scWAT CLOCK
r = 0.4252
p = 0.0485
Circulating leptin (µg/L)

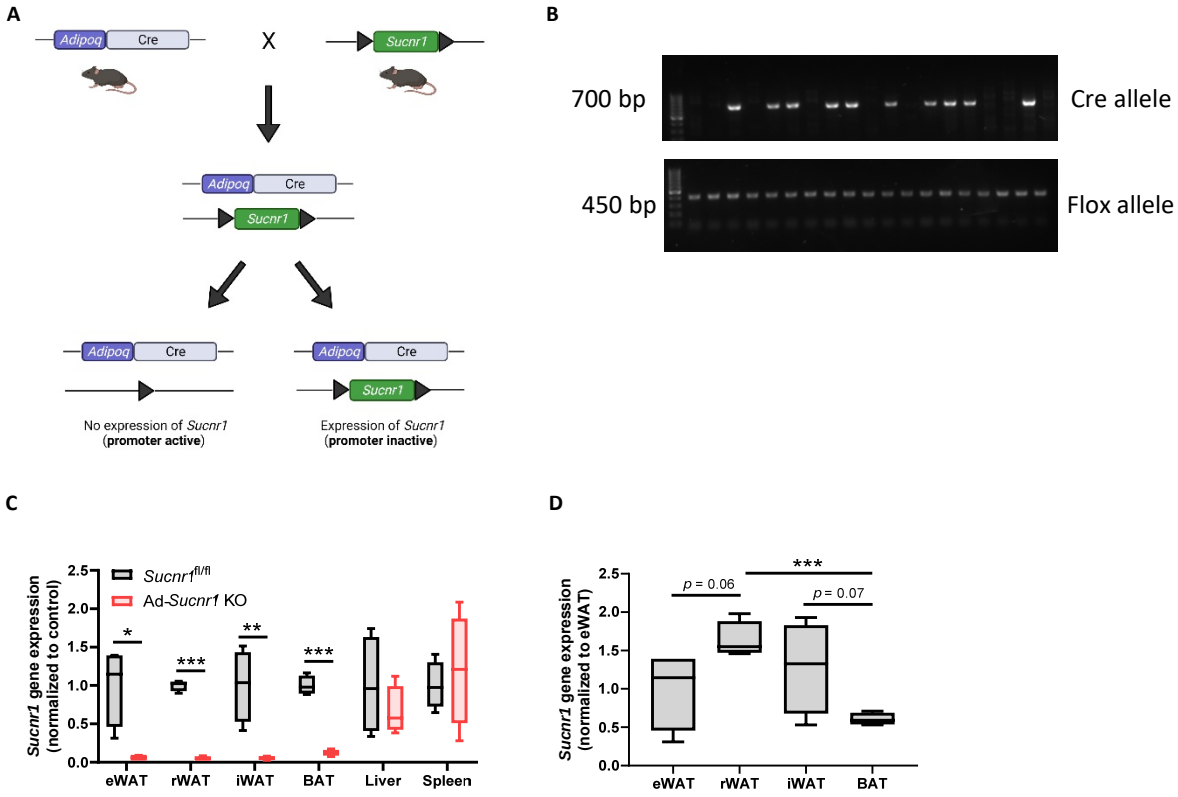

Figure S1. Generation of adipocyte-specific deletion of *Sucnr1* in mice. (Related to Figure 1) (A) Generation and **(B)** genotyping of *Sucnr1*$^{fl/fl}$ and Ad-*Sucnr1* KO mice (Cre allele=700 bp; Flox allele=450 bp). **(C)** qPCR analysis of *Sucnr1* in eWAT, rWAT, iWAT, BAT, liver, and spleen in Ad-*Sucnr1* KO mice and in age-matched *Sucnr1*$^{fl/fl}$ littermates (n=3–4/group). **(D)** *Sucnr1* expression in eWAT, rWAT, iWAT, and BAT in *Sucnr1*$^{fl/fl}$ mice (n=4 mice/tissue). Data are presented as box and whiskers plots showing median, first and third quartiles and maximum and minimum values; * $p<0.05$, ** $p<0.01$; *** $p<0.001$ (Unpaired *t*-test in bar graphs).

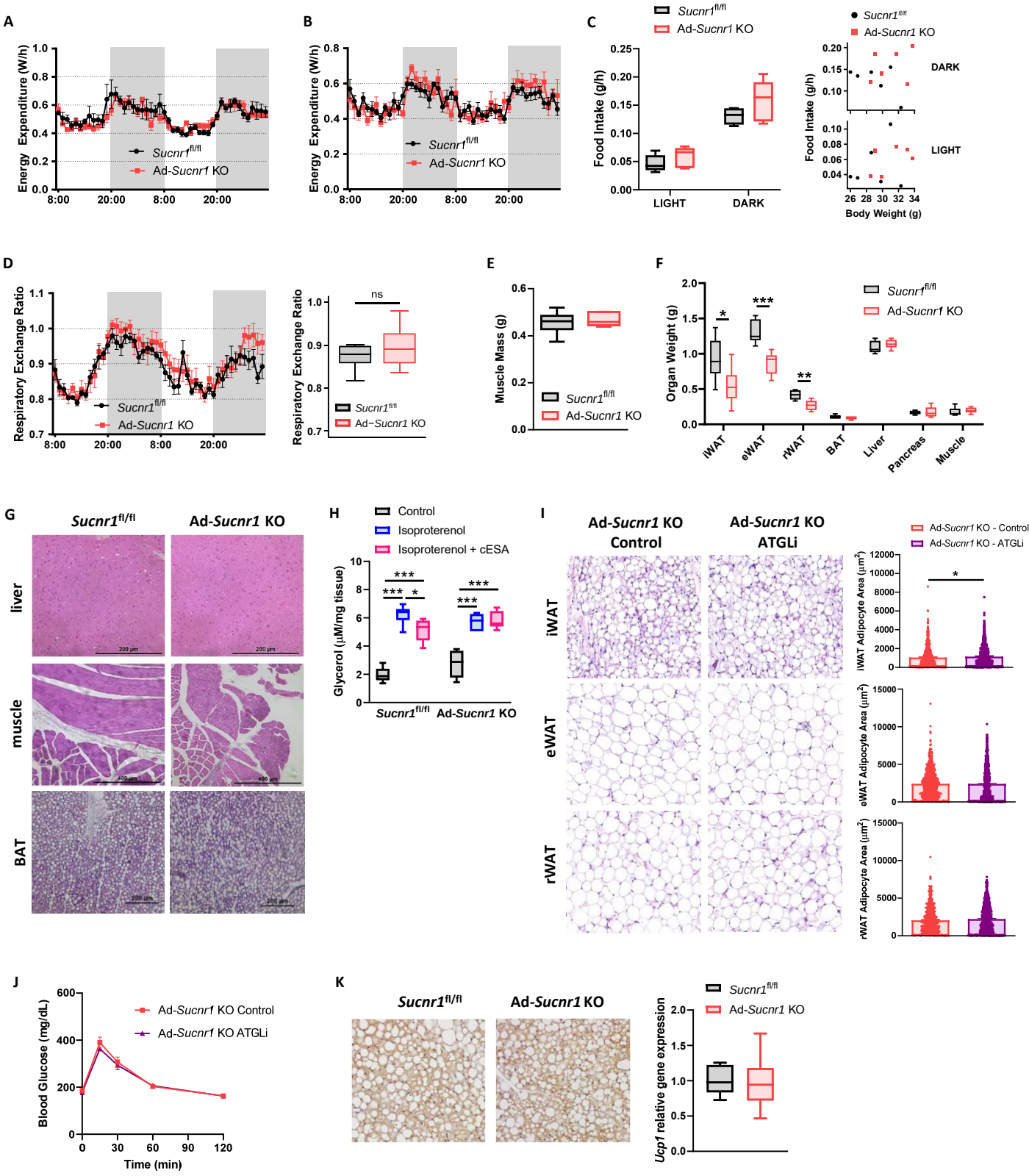
A
Energy Expenditure (W/h)
Sucnr1fl/fl
Ad-Sucnr1 KO
8:00
20:00
B
C
Food Intake (g/h)
LIGHT
DARK
Body Weight (g)
D
Respiratory Exchange Ratio
ns
E
Muscle Mass (g)
F
Organ Weight (g)
iWAT
eWAT
rWAT
BAT
Liver
Pancreas
Muscle
G
liver
muscle
BAT
H
Control
Isoproterenol
Isoproterenol + cESA
Glycerol (μM/mg tissue)
I
Ad-Sucnr1 KO Control
Ad-Sucnr1 KO ATGLi
Ad-Sucnr1 KO - Control
Ad-Sucnr1 KO - ATGLi
iWAT Adipocyte Area (μm2)
eWAT Adipocyte Area (μm2)
rWAT Adipocyte Area (μm2)
J
Blood Glucose (mg/dL)
Time (min)
K
Ucp1 relative gene expression

Figure S2. Metabolic phenotype of mice with conditional adipocyte deletion of *Sucnr1*. (Related to Figure 1). (A) EE at 12 weeks of life (ANCOVA, weight p=0.008 and genotype p=0.152). **(B)** EE (ANCOVA, weight p=0.875 and genotype p=0.549); **(C)** food intake during light and dark hours (left) and regression-based plot of food intake and body weight as covariate (right) (ANCOVA, genotype p=0.881 and 0.139 in light and dark respectively); and **(D)** RER (ANOVA, p=0.345 at week 20 of life (n=6 *Sucnr1*$^{fl/fl}$; n=6 Ad-*Sucnr1* KO). **(E)** qMRI quantification of muscle mass (n=8 *Sucnr1*$^{fl/fl}$; n=6 Ad-*Sucnr1* KO) at week 12 of life. **(F)** Organ weight at 29 weeks (n=5–6 mice/group). **(G)** Representative H&E staining of liver, muscle, and BAT. **(H)** Determination of lipolysis in eWAT explants from *Sucnr1*$^{fl/fl}$ and Ad-*Sucnr1* KO mice, measuring glycerol released in the absence or presence of isoproterenol and *c*ESA (n=6). **(I)** Representative H&E staining of iWAT, eWAT, and rWAT; quantification of adipocyte area; and **(J)** GTT in Ad-*Sucnr1* KO mice treated with ATGLi or vehicle (corn oil) for 2 weeks (n=3 mice/group). **(K)** Representative images of UCP1 immunohistochemistry, and *Ucp1* relative gene expression in BAT (n=5 *Sucnr1*$^{fl/fl}$; n=6 Ad-*Sucnr1* KO). Data are presented as box and whiskers plots showing median, first and third quartiles and maximum and minimum values, or as mean±SEM; * p<0.05; ** p<0.01; *** p<0.001 (Unpaired *t*-test, Mann-Whitney test, or one-way ANOVA in box and whiskers graphs and two-way ANOVA in **J**).

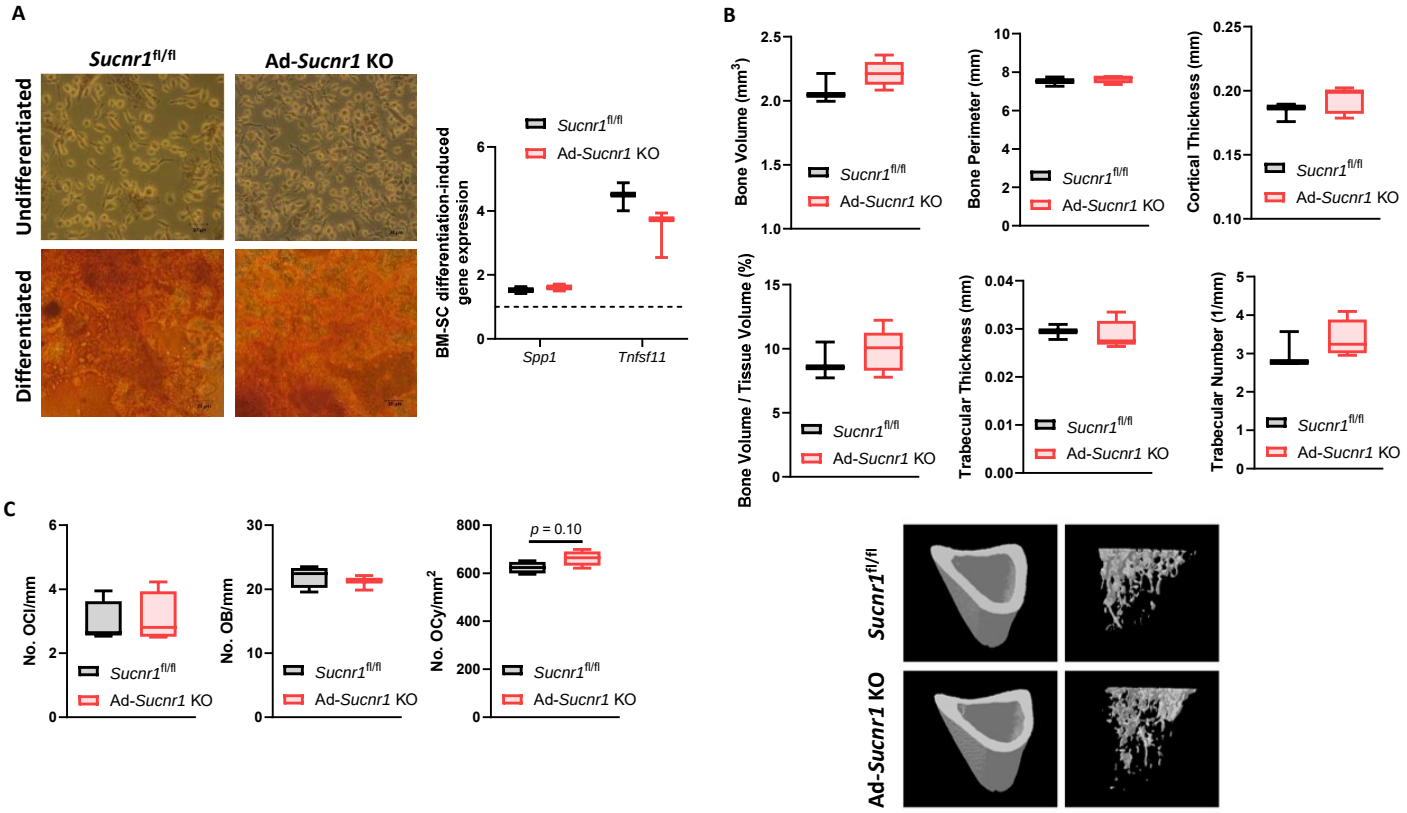

Figure S3. Bone mass phenotype in mice with conditional adipocyte deletion of *Sucnr1* on high-fat diet. (Related to Figure 3) (A) Representative images of Alizarin red S staining of undifferentiated and differentiated bone marrow-mesenchymal stem cells from *Sucnr1*$^{fl/fl}$ and Ad-*Sucnr1* KO mice; and fold change of osteogenesis markers gene expression induced by differentiation (n=3). **(B)** Microcomputed tomography analysis and representative images of cortical and trabecular tibia (n=3 *Sucnr1*$^{fl/fl}$; n=5 Ad-*Sucnr1* KO); and **(C)** quantification of the number of osteoclasts (Ocl), osteoblasts (OB), and osteocytes (Ocy) (n=3–4/group) of *Sucnr1*$^{fl/fl}$ and Ad-*Sucnr1* KO mice fed HFD for 12 weeks. Data are presented as box and whisker plots showing median, first and third quartiles and maximum and minimum values (Unpaired *t*-test or Mann-Whitney test).

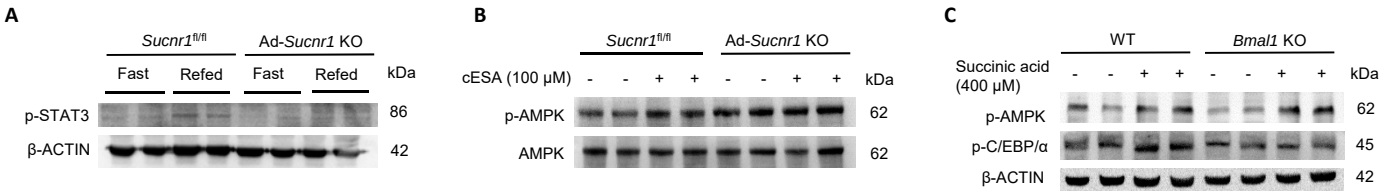

Figure S4. Signalling pathways regulated by fasted-to-fed transition and SUCNR1 activation. (Related to Figures 4, 5, and 6). (A) Representative immunoblot images of p-STAT3 in hypothalamus from *Sucnr1*$^{fl/fl}$ and Ad-*Sucnr1* KO mice in fasted and refed. β-ACTIN was used as a loading control (n=2). **(B)** Representative immunoblot images of p-AMPK in WAT explants from *Sucnr1*$^{fl/fl}$ and Ad-*Sucnr1* KO mice treated with cESA. Total AMPK was used as a loading control (n=2). **(C)** Representative immunoblot images of phosphorylated kinases in iWAT explants from WT and Bmal1 KO mice treated with succinic acid. β-ACTIN was used as a loading control (n=2).

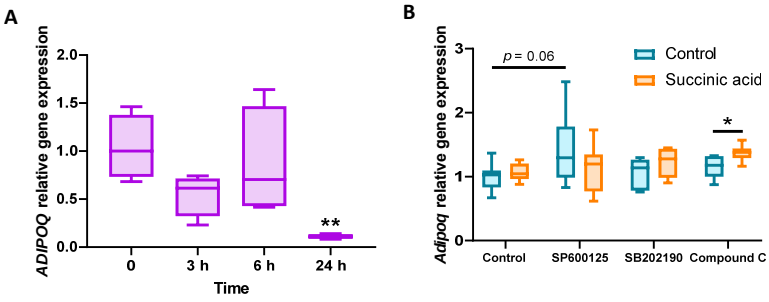

Figure S5. Succinate-SUCNR1 signaling does not control adiponectin expression. (Related to Figure 5) (A) *ADIPOQ* relative gene expression in hASCs treated with 100 μM *c*ESA (n=4). **(B)** *Adipoq* relative gene expression in differentiated 3T3-L1 cells treated with inhibitors of JNK (SP600125), p38 MAPK (SB202190), or AMPK (compound C), and co-treated with 400 μM succinic acid for 3 h (n=6–9). Data are presented as box and whiskers plots showing median, first and third quartiles and maximum and minimum values. * p <0.05; ** p<0.01 (one-way ANOVA followed by Dunnett's multiple comparisons test *vs* control or Unpaired *t*-test).

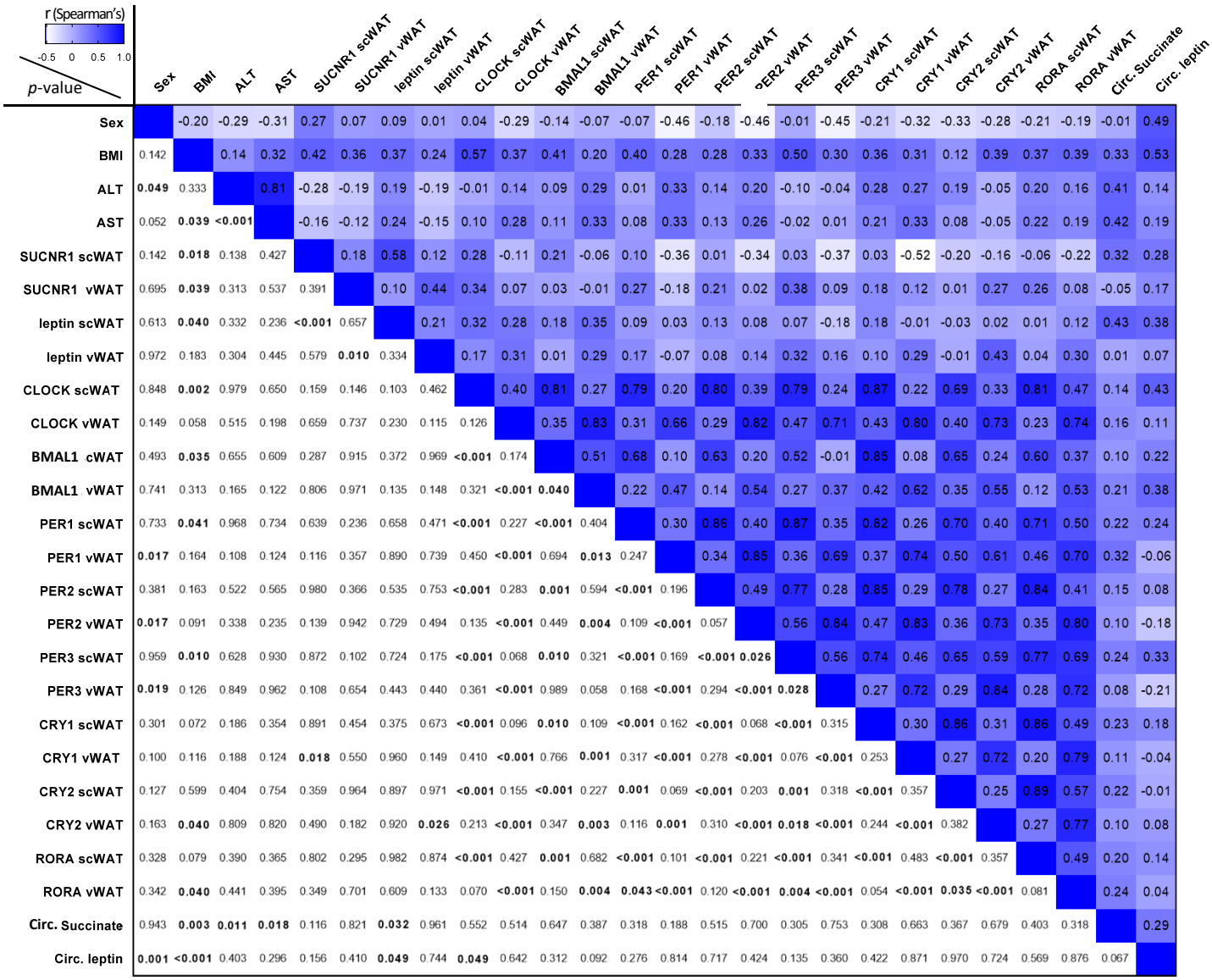

Figure S6. Spearman's correlation matrix between clinical, biochemical, and gene expression variables of the human cohort (Related to Figure 7). The variables depicted only include the significant correlations determined for the biochemical and gene expression variables in Figure 6a. Spearman correlation coefficients and *p*-values are reported for the pairing of variables indicated on the y-axis *vs*. x-axis. Color scale ranges from white (r = −0.5) to blue (r = 1). *P*-values <0.05 were considered to be statistically significant. Abbreviations: ALT, alanine aminotransferase; AST, aspartate aminotransferase; BMAL1, brain and muscle aryl hydrocarbon receptor nuclear translocator-like protein 1; BMI, body mass index; Circ. leptin; circulating leptin; Circ. Succinate, circulating succinate; CLOCK, circadian locomotor output cycles kaput; CRY, cryptochrome; PER, period; RORA, retinoic acid receptor-related orphan receptor alpha; scWAT, subcutaneous white adipose tissue; SUCNR1, succinate receptor 1; vWAT, visceral white adipose tissue.

Table S1 – RNAseq differential gene expression of epididymal white adipose tissue from Ad-*Sucnr1* KO vs *Sucnr1*$^{fl/fl}$ mice. Adjusted *p*-value <0.05.

(Related to Figure 6).

	Symbol	Entrez	Fold change.shrinked	Adjusted *p*-value
Up-regulated genes	*Gm24382*	115489788	34.308	0.0001
	Zfp949	71640	2.637	< 0.0001
	Gsta4	14860	2.469	< 0.0001
	Sh2b2	23921	1.904	0.0002
	Tmem179	104885	1.904	0.0012
	Lrrc15	74488	1.898	0.0069
	6430571L13Rik	235599	1.857	0.0042
	Vwc2	319922	1.829	0.0020
	Ciart	229599	1.828	0.0003
	Cd164l2	69655	1.810	0.0020
	Syde2	214804	1.771	0.0003
	Mc5r	17203	1.665	0.0113
	Tef	21685	1.626	< 0.0001
	Per3	18628	1.621	< 0.0001
	Klf15	66277	1.619	0.0020
	Dbp	13170	1.614	0.0018
	Col6a6	245026	1.580	0.0016
	Pcsk4	18551	1.556	0.0062
	Gpd1	14555	1.535	0.0126
	Per1	18626	1.530	0.0018
	Lrp12	239393	1.528	0.0025
	Ppargc1b	170826	1.516	0.0006
	Per2	18627	1.504	0.0012
	B630019A10Rik	105246089	1.492	0.0191
	Gpr135	238252	1.491	0.0074
	Adora1	11539	1.466	0.0077
	Slc36a2	246049	1.460	0.0246
	Dcun1d3	233805	1.454	0.0010
	Hif3a	53417	1.443	0.0300
	Fam117a	215512	1.425	0.0010
	Myorg	329828	1.420	0.0104
	Cpn2	71756	1.418	0.0204
	Gys1	14936	1.403	0.0170
	Acsl1	14081	1.403	0.0259
	Tob2	57259	1.401	0.0006
	C730002L08Rik	320155	1.396	0.0306
	Rgma	244058	1.387	0.0204
	A530016L24Rik	319942	1.386	0.0317
	Kctd6	71393	1.370	0.0088
	Ppara	19013	1.366	0.0364
	Sccpdh	109232	1.364	0.0321
	Mlxipl	58805	1.361	0.0025
	Bcat2	12036	1.344	0.0187
	Lpin1	14245	1.343	0.0407
	Nr1d2	353187	1.339	< 0.0001
	Gm36210	102640043	1.339	0.0384
	Oscp1	230751	1.334	0.0392
	Ranbp9	56705	1.332	0.0236
	Fam214a	235493	1.331	0.0418
	Prodh	19125	1.329	0.0321
	Txnrd3	232223	1.325	0.0246
	4933406C10Rik	74076	1.320	0.0316
	Arl4a	11861	1.319	0.0418
	Gys2	232493	1.313	0.0433
	Gm34408	102637649	1.308	0.0349
	Rfc4	106344	1.296	0.0277
	Pard6g	93737	1.295	0.0418
	Fbxo3	57443	1.287	< 0.0001
	Eif4a2	13682	1.285	0.0010
	Hemk1	69536	1.281	0.0042
	Micall1	27008	1.279	0.0046
	Tmem53	68777	1.278	0.0494
	Ing2	69260	1.269	0.0012
	Clcn2	12724	1.276	0.0635
	Lonrf1	244421	1.260	0.0294

Table S1 (continued)

	Symbol	Entrez	Fold change.shrinked	Adjusted *p*-value
Down-regulated genes	*Lcp1*	18826	-1.251	0.0364
	Srp54b	665155	-1.256	< 0.0001
	Srp54a	24067	-1.257	< 0.0001
	Itm2c	64294	-1.266	0.0277
	Selp	20344	-1.269	0.0499
	Atoh8	71093	-1.269	0.0499
	Mthfsl	100039707	-1.272	0.0150
	Dll1	13388	-1.292	0.0282
	Slc7a7	20540	-1.300	0.0069
	Rims1	116837	-1.304	0.0279
	Cnn1	12797	-1.312	0.0277
	Ifi44	99899	-1.320	0.0465
	Plvap	84094	-1.328	0.0232
	Etl4	208618	-1.329	0.0279
	Lpcat2	270084	-1.344	0.0413
	Dusp4	319520	-1.347	0.0346
	Arhgap20	244867	-1.355	0.0010
	Mall	228576	-1.371	0.0277
	Adm	11535	-1.384	0.0057
	Srprb	20818	-1.391	< 0.0001
	Foxs1	14239	-1.394	0.0235
	Gm47283	170942	-1.396	0.0087
	Akr1b7	11997	-1.437	0.0171
	Gm13710	672763	-1.446	0.0012
	Gm7972	666190	-1.453	0.0289
	Mapkapk3	102626	-1.458	0.0205
	Pcdh12	53601	-1.543	0.0130
	Sh3bgrl2	212531	-1.545	0.0018
	Ier5	15939	-1.607	0.0017
	Abhd14b	76491	-1.677	< 0.0001
	Spon2	100689	-1.772	0.0039
	Ppm1m	67905	-2.060	< 0.0001
	Cldn5	12741	-2.072	< 0.0001
	Adamts4	240913	-2.390	< 0.0001
	Arntl	11865	-2.546	< 0.0001
	Rpl29	19944	-3.374	< 0.0001
	Sucnr1	84112	-18.897	< 0.0001
	Ptgs2	19225	-22.624	0.0011

Table S2 – Anthropometric and Biochemical Variables from the Human Cohort. (Related to Figure 7).

Variables	Lean	Obese
n	22	34
Sex (female/male)	17/5	18/16
Age (years)	51.4 ± 15.7	52.3 ± 12.3
BMI (kg/m^2)	22.5 ± 2.0	34.5 ± 3.67***
Glucose (mmol/L)	4.9 ± 0.8	5.3 ± 0.9
Total cholesterol (mmol/L)	4.8 ± 0.7	5.0 ± 1.0
HDLc (mmol/L)	1.6 ± 0.3	1.2 ± 0.3***
LDLc (mmol/L)	2.9 ± 0.6	3.2 ± 0.8
Triglycerides (mmol/L)	0.9 ± 0.4	1.9 ± 1.1***
Insulin (pmol/L)	35.8 ± 12.0	104.8 ± 43.0*
HOMA-IR	1.2 ± 0.6	3.8 ± 1.6*
GGT (µkat/L)	0.9 ± 2.0	2.0 ± 4.6**
ALT (µkat/L)	0.5 ± 0.7	0.5 ± 0.6
AST (µkat/L)	0.3 ± 0.2	0.5 ± 0.4*
Circulating Succinate (µmol/L)	54.8 ± 39.0	102.9 ± 79.0*
Circulating Leptin (µg/L)	10.1 ± 7.6	27.7 ± 21.9***

Abbreviations: ALT, Alanine Aminotransferase; AST, Aspartate Aminotransferase; BMI, body mass index; GGT, Gamma Glutamyltransferase; LDLc, low-density lipoprotein cholesterol; HDLc, high-density lipoprotein cholesterol; HOMA-IR, Homeostatic Model Assessment for Insulin Resistance. Results are expressed as mean ± SD. * *p*-value <0.05; ** *p*-value <0.01; and *** *p*-value <0.001 (Unpaired *t*-test or Mann-Whitney test).

Table S3 – Regressions Coefficients for predicting circulating leptin levels. (Related to Figure S6).

Circulating leptin (R=0.812; R^2=0.660)					
	B (non-standardized)	**SE**	**95% CI**	**Beta (standardized)**	***p*-value**
Constant	-37.501	11.293	-60.863 – -14.139	-	<0.01
Sex	17.841	3.802	9.976 – 25.705	0.584	<0.001
BMI	0.831	0.313	0.184 – 1.478	0.359	<0.05
***LEP* scWAT**	2.261	1.078	0.030 – 4.491	0.286	<0.05

Variables included in the model: age, glucose, body mass index (BMI), and *LEP* expression in subcutaneous white adipose tissue (scWAT).

Table S4 – Regressions Coefficients for predicting *LEP* expression in human subcutaneous adipose tissue. (Related to Figure S6).

***LEP* expression in scWAT (R=0.487; R^2=0.544)**					
	B (non-standardized)	**SE**	**95% CI**	**Beta (standardized)**	***p*-value**
Constant	2.986	1.185	0.521-5.451	-	0.020
***SUCNR1* scWAT**	0.434	0.149	0.124-0.743	0.450	<0.01
Circulating Leptin	0.058	0.020	0.017-0.098	0.454	<0.01
Age	-0.050	0.021	-0.094-0.006	-0.353	0.029

Variables included in the model: Body mass index, sex, circulating succinate, *SUCNR1* expression in human subcutaneous white adipose tissue (scWAT), circulating leptin, and age.

Table S5 – Regressions Coefficients for predicting *LEP* expression in human visceral adipose tissue. (Related to Figure S6).

***LEP* expression i vWAT (R=0.470; R^2=(.221)**					
	B (non-standardized)	**SE**	**95% CI**	**Beta (standardized)**	***p*-value**
Constant	0.868	0.235	0.388-1.348	-	<0.001
***SUCNR1* vWAT**	0.277	0.095	0.083-0.471	0.470	<0.01

Variables included in the model: age, sex, and *SUCNR1* expression in visceral white adipose tissue (vWAT).

Table S6 – Taqman Gene Expression Assay References. (Related to STAR Methods).

Gene Name	Mouse	Human
B2m	Mm00437762_m1	
RNA18S5		Hs03928985_g1
Sucnr1* / *SUCNR1	Mm02620543_s1	Hs00908230_m1
Lep* / *LEP	Mm00434759_m1	Hs00174877_m1
Adipoq* / *ADIPOQ	Mm00456425_m1	Hs00605917_m1
Ucp1	Mm01244861_m1	
Cidea	Mm00432554_m1	
Tnfsf11	Mm00441906_m1	
Spp1	Mm00436767_m1	
Npy	Mm01410146_m1	
Agrp	Mm00475829_g1	
Pparg	Mm00440940_m1	
Fasn	Mm00662319_m1	
Slc2a4	Mm00436615_m1	
Bmal1* / *BMAL1	Mm00500223_m1	Hs00154147_m1
CLOCK		Hs00231857_m1
Rora* / *RORA	Mm01173766_m1	Hs00536545_m1
Per1* / *PER1	Mm00501813_m1	Hs00242988_m1
Per2* / *PER2	Mm00478099_m1	Hs00256143_m1
Per3* / *PER3	Mm00478120_m1	Hs00213466_m1
CRY1		Hs00172734_m1
CRY2		Hs00323654_m1